The Astronomical Journal, 124:1528–1554, 2002 September

BVI TIME-SERIES DATA OF THE GALACTIC GLOBULAR CLUSTER NGC 3201. I. RR LYRAE STARS[1]

A. M. Piersimoni,[2] G. Bono,[3] and V. Ripepi[4]

Received 2002 February 19; accepted 2002 May 13

ABSTRACT

We present Johnson *BV*- and Kron-Cousins *I*-band time-series data collected over three consecutive nights in a region of 13 arcmin^2 centered on the Galactic globular cluster (GGC) NGC 3201. The time sampling of current CCD data allowed us to derive accurate light curves and, in turn, mean magnitudes and colors for a sample of 53 RR Lyrae stars. To overcome the thorny problem of differential reddening affecting this cluster, we derived new empirical relations connecting the intrinsic $B-V$ and $V-I$ colors of fundamental (RR*ab*) RR Lyrae stars to the luminosity amplitude, the metallicity, and the pulsation period. The key features of these relations are the following: (1) they rely on stellar parameters, which are not affected by reddening; (2) they supply accurate estimates of intrinsic colors across the fundamental instability strip and cover a wide metallicity range; (3) they were derived by neglecting the RR Lyrae stars that are affected by amplitude modulation. Moreover, the zero point of the $E(B-V)$ reddening scale was empirically checked using the large sample of RR Lyrae stars in M3 from Corwin & Carney, a GGC affected by a vanishing reddening. According to these relations we estimated individual reddenings for RR Lyrae stars in our sample and the main results we found are the following: (1) The mean cluster reddening based on $E(B-V)$ color excesses is $\langle E(B-V)\rangle = 0.30 \pm 0.03$. This estimate is slightly higher than the mean reddening evaluations available in the literature or based on the dust infrared map by Schlegel, Finkbeiner, & Davis, i.e., $\langle E(B-V)\rangle = 0.26 \pm 0.02$. Note that the angular resolution of this map is $\approx 6'$, whereas for current reddening map it is $\approx 1'$. (2) The mean cluster reddening based on $E(V-I)$ color excesses is $\langle E(V-I)\rangle = 0.36 \pm 0.05$. This estimate is only marginally in agreement with the mean cluster reddening obtained using the reddening map by von Braun & Mateo and derived by adopting cluster turnoff stars, i.e., $\langle E(V-I)\rangle = 0.25 \pm 0.07$. On the other hand, current intrinsic spread among individual reddenings ($\approx$0.2 mag) agrees quite well with the estimate provided by previous authors. It is noteworthy that previous mean cluster reddenings are in very good agreement with values obtained using the empirical relations for intrinsic RR Lyrae colors provided by Kovacs & Walker. (3) According to current individual $E(B-V)$ and $E(V-I)$ reddenings and theoretical predictions for horizontal-branch stars, we found that the true distance modulus for this cluster is 13.32 ± 0.06 mag. This determination is somehow supported by the comparison between predicted and empirical pulsation amplitudes. (4) The comparison between present luminosity amplitudes and estimates available in the literature discloses that approximately 30% of fundamental RR Lyrae stars are affected by amplitude modulation (the Blazhko effect). This finding confirms empirical evidence originally brought out by Szeidl and by Smith.

Key words: globular clusters: individual (NGC 3201) — RR Lyrae variable — stars: evolution — stars: horizontal-branch — stars: oscillations

1. INTRODUCTION

The stellar content of Galactic globular clusters (GGCs) plays a crucial role in our understanding of the evolutionary properties of old, low-mass stars. Even though pioneering observational investigations on these fascinating objects appeared more than 50 years ago, complete and homogeneous color-magnitude diagrams (CMDs) for both bright and very faint stars became available only recently in the literature. The accuracy of photometric data is a key ingredient for providing reliable estimates of observables to be compared with evolutionary predictions. A paramount observational effort has been devoted to horizontal branch (HB) stars and in particular to RR Lyrae variables, since these objects are fundamental primary distance indicators in the Galaxy and in Local Group galaxies. Moreover and even more importantly, the RR Lyrae distance scale is often used for estimating the turnoff (TO) luminosity and, in turn, the age of GGCs (Vandenberg, Stetson, & Bolte 1996; Cassisi et al. 1998; Caputo 1998). This means that cluster data relying on the same photometric zero point can supply more robust age determinations (Rosenberg et al. 1999, 2000).

During the last few years, several thorough investigations have been aimed at improving the accuracy of both evolutionary and pulsational predictions. New sets of full amplitude, nonlinear RR Lyrae models have been constructed, which include a nonlocal, time-dependent treatment of convective transport, and, in turn, a self-consistent approach to the coupling between pulsation and convection (Bono & Stellingwerf 1994; Bono et al. 1997c; Feuchtinger 1999, and references therein). In contrast to linear and nonlinear radiative models this new approach provided homogeneous sets

[1] Based on observations collected at the European Southern Observatory, La Silla, Chile.

[2] Osservatorio Astronomico di Collurania, via Maggini, I-64100 Teramo, Italy; piersimoni@te.astro.it.

[3] Osservatorio Astronomico di Roma, via Frascati 33, I-00040 Monte Porzio Catone, Italy; bono@mporzio.astro.it.

[4] Osservatorio Astronomico di Capodimonte, via Moiariello 16, I-80131 Napoli, Italy; ripepi@na.astro.it.

of theoretical observables—modal stability, pulsational amplitudes—for both fundamental and first-overtone pulsators to be compared with actual properties of RR Lyrae stars. Moreover, the pulsation models, to account for the behavior of RR Lyrae stars in GGCs and in the Galactic field, were constructed by adopting stellar masses and luminosities predicted by evolutionary models over a wide metallicity range ($0.0001 \leq Z \leq 0.04$, Bono et al. 1997a, 1997b, 1997c). At the same time, evolutionary models experienced substantial improvements in the input physics, such as radiative opacities and equation of state (D'Antona, Caloi, & Mazzitelli 1997; Vandenberg & Irwin 1997; Cassisi et al. 1998) and the inclusion of atomic diffusion (Cassisi et al. 1999). The reader interested in a detailed discussion of the impact of these new physical ingredients on theoretical observables is referred to the comprehensive reviews by Vandenberg et al. (1996), Caputo (1998), and Castellani (1999).

On the other hand, several recent observational investigations performed by adopting CCD cameras on relatively small telescopes disclosed that current samples of variable stars in GGCs are far from being complete. In fact, a large accumulation of evidence suggests that CCD observations of the innermost cluster regions allowed the identification of sizable samples of binary systems (Albrow et al. 2001; Kaluzny & Thompson 2001), exotic objects (Edmonds et al. 2002), and oscillating blue stragglers (Kaluzny, Olech, & Stanek 2001 and references therein), as well as a substantial increase in the sample of cluster RR Lyrae variables (Walker & Nemec 1996; Walker 1998; Caputo et al. 1999; Olech et al. 2001).

Finally, we mention that new data reduction techniques, such as the image subtraction method (Alard 1999, 2000), when compared with profile fitting methods, supply not only a substantial increase in the number of variable stars detected in crowded regions (Olech et al. 1999) but also an improvement in the photometric accuracy of light curves.

Obviously, the accuracy of astrophysical parameters, such as stellar masses and luminosities based on comparison between theory and observations, does not depend only on the accuracy of empirical data but also on the size of individual samples. As a consequence, GGCs that present a relatively large number of RR Lyrae variables can provide tight constraints on the evolutionary and pulsational behavior of these objects. Keeping in mind this caveat, we collected new multiband time-series CCD data of the GGC NGC 3201. The main reason we selected this cluster is that it will supply a comprehensive analysis of a large sample of RR Lyrae stars ($N_{\rm RR} = 77$, Clement et al. 2001) in an Oosterhoff type I (Oo I) cluster. Moreover, up to now only photographic light curves of RR Lyrae stars in NGC 3201 have been available in the literature (Cacciari 1984, hereafter C84).

This cluster is located close to the Galactic plane ($l_{\rm II} = 277.228$, $b_{\rm II} = 8.641$) and it is a valuable target for spectroscopic surveys because of its proximity (DM ≈ 13.32 mag) and its relatively low central concentration [log $\rho_0 = 2.69$ ($L_\odot$ /pc^3), Trager, Djorgovski, & King 1993]. A further interesting feature of NGC 3201 is that it presents a retrograde orbit (van den Bergh 1993), thus suggesting that it is not a typical member of the halo GC population. The main drawbacks of NGC 3201 are that it is affected by field contamination, presents a relatively high reddening [$\langle E(B-V)\rangle \approx 0.25-0.30$], and is also affected by differential reddening. The most recent CCD photometric studies of this cluster have been provided by Alcaino, Liller, & Alvarado (1989, *BVRI* bands), Brewer et al. (1993, *UBV* bands), Covino & Ortolani (1997, *BV* data, hereafter CO97). More recently Rosenberg et al. (2000) and von Braun & Mateo (2001, hereafter vBM01) collected deep and accurate *VI* data.

This is the first paper of a series devoted to the evolutionary and pulsation properties of stellar population in NGC 3201. In § 2 we present the observations and the strategy adopted to reduce the data together with the calibration of the photometric zero point and the comparison with previous investigations available in the literature. A brief discussion of the most recent metallicity determinations of NGC 3201 is presented in § 3. The pulsational parameters and the light curves of fundamental and first-overtone (FO) RR Lyrae stars are discussed in § 4, while § 4.1 deals with variables showing amplitude modulation (the Blazhko effect). In § 5 we present a detailed analysis of individual reddening evaluations for RR Lyrae stars according to $B-V$ and $V-I$ colors (§§ 5.1 and 5.2), as well as to the Fourier parameters of *V*-band light curves (§ 5.3). In particular, in the first two subsections we discuss three new empirical relations connecting the intrinsic color of RR*ab* stars with luminosity amplitude, pulsation period, and metallicity. The comparison between these relations and similar relations available in the literature are also described in this section. The comparison between theoretical observables and empirical data is detailed in § 6. In this section we briefly discuss the comparison of RR Lyrae stars in NGC 3201 with the sample of RR Lyrae stars in IC 4499 and in M5. The main features of the CMD are outlined in § 7. In this section we also present the (V, $B-V$) and the (V, $V-I$) CMDs dereddened by means of the reddening map derived using current sample of RR*ab* stars. The main results of this investigation are summarized in § 8, together with the future developments of this project. Finally, in the Appendix we list a series of comments on individual variables.

2. OBSERVATIONS AND DATA REDUCTION

Multiband photometric data were collected with the 1.5 m Danish telescope at ESO-La Silla equipped with a Loral CCD (2024 × 2024 pixels) during an observing run from 1996 February 21–23. The field of view of the CCD is $13' \times 13'$, and NGC 3201 was approximately centered on this field. The exposure times were 180 s for the *B* band and 40 s for both *V* and *I* bands, respectively. We roughly collected 80 frames per band, and the stars were identified and measured by using DAOPHOT and ALLSTAR packages (Stetson 1987, 1995). The internal accuracy of our photometry is of the order of hundredths of magnitude at the typical magnitude of RR Lyrae stars. However, the sensitivity of the CCD drastically decreases in the 300 pixels ($\approx 1\rlap{.}'9$) close to the edges. As a consequence, the S/N ratio of the stars located in this region is significantly lower and the light curves of RR Lyrae variables such as V7, V48, V51, and V71 present a larger scatter.

Oddly enough, the absolute calibration of current data has been a pleasant experience, since Stetson (2000)[5] collected a sizable sample of local standards across NGC 3201.

[5] Data available at http://cadcwww.hia.nrc.ca/standards.

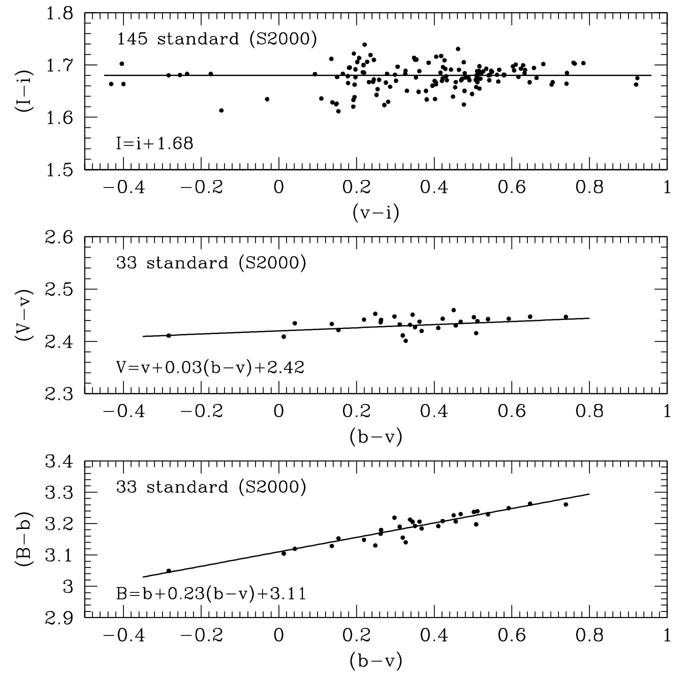

FIG. 1.—Instrumental magnitudes as a function of the instrumental $V-I$ (*top*) and $B-V$ (*middle*, *bottom*) color. Instrumental magnitudes were transformed into standard *BVI* magnitudes according to the photometric data collected by Stetson (2000) that are available at http://cadcwww.hia.nrc.ca/standards.

On the basis of these new standards it has been possible to derive an accurate calibration, since V and I standards (145 stars) cover a region of $4'.5 \times 4'.5$ around the center of the cluster, while the standards in B (33 stars) are distributed over a region of $\sim 2'.6 \times 2'.6$. Moreover, it is noteworthy that the $B-V$ color of the standards range from 0.35 to 1.55, while the $V-I$ colors range from 0.2 to 1.7. This means that current calibration properly covers both blue/extreme HB stars as well as stars close to the tip of the red giant branch (RGB). Figure 1 shows the calibration equations we derived according to the difference between current instrumental magnitudes and the Stetson's standards. On the basis of this comparison we estimate that our calibration errors are of the order of 0.02 mag in V and B bands and of 0.03 mag in the I band. The uncertainty in the I band is larger than in the B, V bands. The difference might be due to the limited accuracy of the flat fields in the former band. As a matter of fact, the uniform illumination required for flat fields could not be properly accomplished in focal reducer instruments because of scattered light and sky concentration. Moreover, this effect can be wavelength dependent (Andersen, Freyhammer, & Storm 1995). In particular, we find that the I magnitudes in the two CCD regions located at $x > 1300$ and $y < 600$ pixels are less accurate, and indeed in these regions the scatter between current and Stetson's magnitudes is larger.

As a further and independent test of the intrinsic accuracy of current calibration, we compared our (V, $V-I$) CMD with the CMD recently provided by Rosenberg et al. (2000)[6] and our (V, $B-V$) CMD with the CMD provided by CO97.

[6] Data available at http://menhir.pd.astro.it.

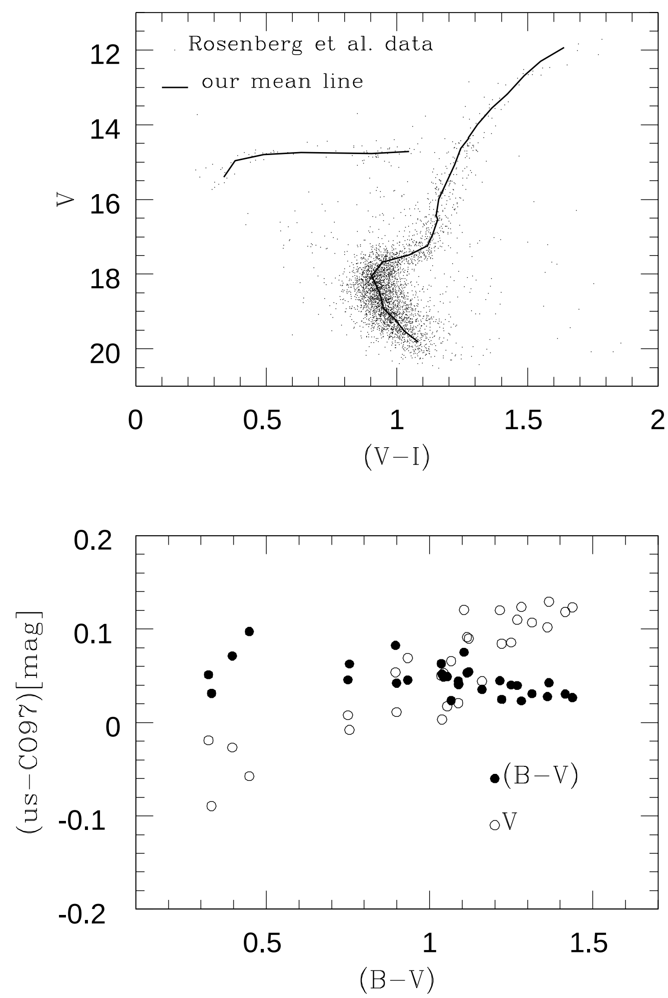

FIG. 2.—*Top*: Comparison between the (V, $V-I$) CMD provided by Rosenberg et al. (2000) and the current cluster mean line. *Bottom*: Difference between present V magnitudes (*open circles*) and $B-V$ colors (*filled circles*) for a sample of bright stars in common with CO97.

The top panel of Figure 2 shows that our data are in very good agreement with the Rosenberg et al. data, and indeed the main branches of the CMD nicely overlap. This evidence is further supported by the fact that both the magnitude ($V_{\rm TO} = 18.2$ mag) and the color [$(V-I)_{\rm TO} = 0.905$] of the turnoff estimated by Rosenberg et al. are, within current uncertainties, in remarkable agreement with our evaluations.

As far as the *BV* data is concerned, we found that the mean loci provided by CO97 seem slightly bluer than our diagram, and therefore we decided to check this discrepancy on a star by star basis. The bottom panel of Figure 2 shows the difference in magnitude (*open circles*) and color (*filled circles*) between our and CO97's HB and RGB stars. Data plotted in this panel clearly show a color offset that ranges from $\sim$0.02 mag for red objects to $\sim$0.05 mag for blue objects. On the other hand, the difference in the V magnitude steadily increases from blue to red objects. We suggest that the difference in the V band could be due to the procedure they adopted to calibrate the bright end of the CMD. In fact, their Danish data set ($V < 16$) was calibrated with the NTT data set, i.e., with photometric data with $16 < V < 18$ and $0.5 < (B-V) < 1$. As a consequence, their color term in the V magnitude calibration was extrapolated and possibly underestimated. This working hypothesis is supported by the fact that the difference in this color range is vanishing. Moreover, our determination of the distance modulus agrees quite well with their evaluation (see § 6).

3. METAL ABUNDANCE

The metal content is a key parameter to assess on a quantitative basis the properties of stellar populations. The mean metallicity of NGC 3201 has been a matter of concern for a long time. In fact, metal abundances based on integrated properties (Zinn 1980; Zinn & West 1984, hereafter ZW84), on low-dispersion spectra, and on the RGB slope in the (V, $V-I$) CMD (Da Costa, Frogel, & Cohen 1981) do suggest for this cluster a mean metallicity similar to M3 and NGC 6752, i.e., [Fe/H] ≈ -1.61. However, Smith & Manduca (1983) found—on the basis of the ΔS method applied to nine RR Lyrae stars—that the mean metallicity is -1.34 ± 0.15. They also found no significant variation in the metal content among the RR Lyrae stars in the sample. On the other hand, Carretta & Gratton (1997 hereafter CG97), by reanalyzing high-dispersion CCD spectra (three stars) and on the basis of updated atmosphere models (Kurucz 1992), found a mean metallicity of [Fe/H] $= -1.23 \pm 0.09$, which is higher than previous ones. A slightly lower metal abundance was estimated by Carney (1996) [Fe/H] $= -1.34$, who also provided an α-element overabundance of $[\alpha/\mathrm{Fe}] = 0.26$.

The discrepancy between different empirical estimates was not solved by the extensive and homogeneous spectroscopic investigation, based on the equivalent width of the Ca II triplet, provided by Rutledge, Hesser, & Stetson (1997). In fact, they found that the metallicity of NGC 3201 ranges from [Fe/H] $= -1.24$ to [Fe/H] $= -1.53$ according to the metallicity scales of CG97 and ZW84, respectively. The empirical scenario was further complicated by the fact that a spread in the metal content has also been suggested (Da Costa et al. 1981). This hypothesis was somehow supported by accurate spectroscopic measurements by Gonzales & Wallerstein (1998, hereafter GW98). They found that metallicity estimates for 17 cluster RG stars range from -1.17 to -1.68 and present variations that are roughly a factor of 4 larger than the typical uncertainty on individual [Fe/H] measurements. This notwithstanding, GW98 suggested that an intrinsic spread in the iron abundance among the RG stars of NGC 3201 is unlikely and provided a mean metal content of -1.42. According to this metal content, to the α-element enhancement estimated by GW98, $[\alpha/\mathrm{Fe}] \simeq 0.40$, and by adopting the Salaris, Chieffi, & Straniero (1993) relation, we estimate that the global metallicity[7] for this cluster is [M/H] $= -1.13$. In the following we will adopt this mean global metallicity and a mean iron abundance of [Fe/H] $= -1.42$.

4. THE RR LYRAE VARIABLES

On the basis of BV-, and I-band data we identified 64 of the 96 variables listed by Sawyer-Hogg (1973, hereafter SH73) and by Samus et al. (1996). We confirm the nonvariability for V33, V70, V74, V75, V81, and V82 quoted by SH73. Seven of the RR Lyrae stars we identified are located in a CCD region where the quality of the photometry is not accurate. Moreover, two out of the eight new suspected variables identified by Lee (1977) and by Welch & Stetson (1993), namely, 2710 and 1405 according to the photometric list by Lee (1977), have been confirmed as "true" variables. According to current photometry the suspected variables—3516, 4702, 2517, 2403—do not show strong evidence of variability, while for 1113 and 1103 we cannot reach any firm conclusion since the quality of the photometry is poor.

We performed a detailed ad hoc search aimed at detecting new RR Lyrae variables, but we did not find any new variables or new candidates. Therefore, according to previous findings the number of RR Lyrae stars and suspected RR Lyrae stars present in NGC 3201 decreases from 104 to 94. Note that SH73 did not detect any variability for V79, a star located close to the tip of the RGB, whereas we found over the three nights a clear variation in the luminosity (see the Appendix for more details).

Our data were collected over three consecutive nights, and therefore the light curves of RR Lyrae variables present a good phase coverage over the full pulsation cycle. The same outcome does not apply to RR Lyrae stars characterized by pulsation periods close to 0.5 days, since they present a poor phase coverage close to maximum/minimum luminosity. Figure 3 shows the atlas of BVI light curves for the entire sample. The old variables were called with the name listed by SH73, while for the new ones we adopted the numbering introduced by Lee (1977). Figure 4 shows B and V light curves for the RR Lyrae stars with a poor phase coverage close to maximum/minimum luminosity. To estimate the mean magnitudes and the amplitudes of these nine objects, we adopted the empirical light-curve template provided by Layden (1998). The solid lines in Figure 4 display the B and V template curves. Note that Layden only provided V band templates, but Borissova, Catelan, & Valchev (2001) found that these light curves, after a proper scaling, can also be adopted to derive the luminosity amplitudes in the B band. Data plotted in Figure 4 show a fair agreement between the template light curves and available empirical data. However, for four (V18, V20, V38, V50) out of the nine variables the B-band data present a systematic difference with the template close to the phase of minimum luminosity. This means that both mean magnitudes, colors, and amplitudes of these variables should be treated with caution since they are affected by larger errors.

As far as the light curves are concerned, the photographic data set collected by C84 is still the most comprehensive and detailed investigation of RR Lyrae stars in NGC 3201. Figure 5 shows the difference in the mean V (*top*) and B (*bottom*) magnitudes between current and C84 estimates. Data plotted in this figure clearly show a very good agreement in the V magnitude, whereas the B magnitudes by C84 are systematically brighter by approximately 0.05–0.075 mag when compared with current estimates. However, such a difference is mainly due to a difference in the zero point of the photometric standards (Lee 1977) adopted by C84. In fact, a detailed comparison between current CCD magnitudes for a dozen of Lee's photographic standards discloses the same shift in the B magnitude.

[7] The global metallicity is a parameter that accounts for both iron and α-element abundances (Carney 1996; Vandenberg 2000).

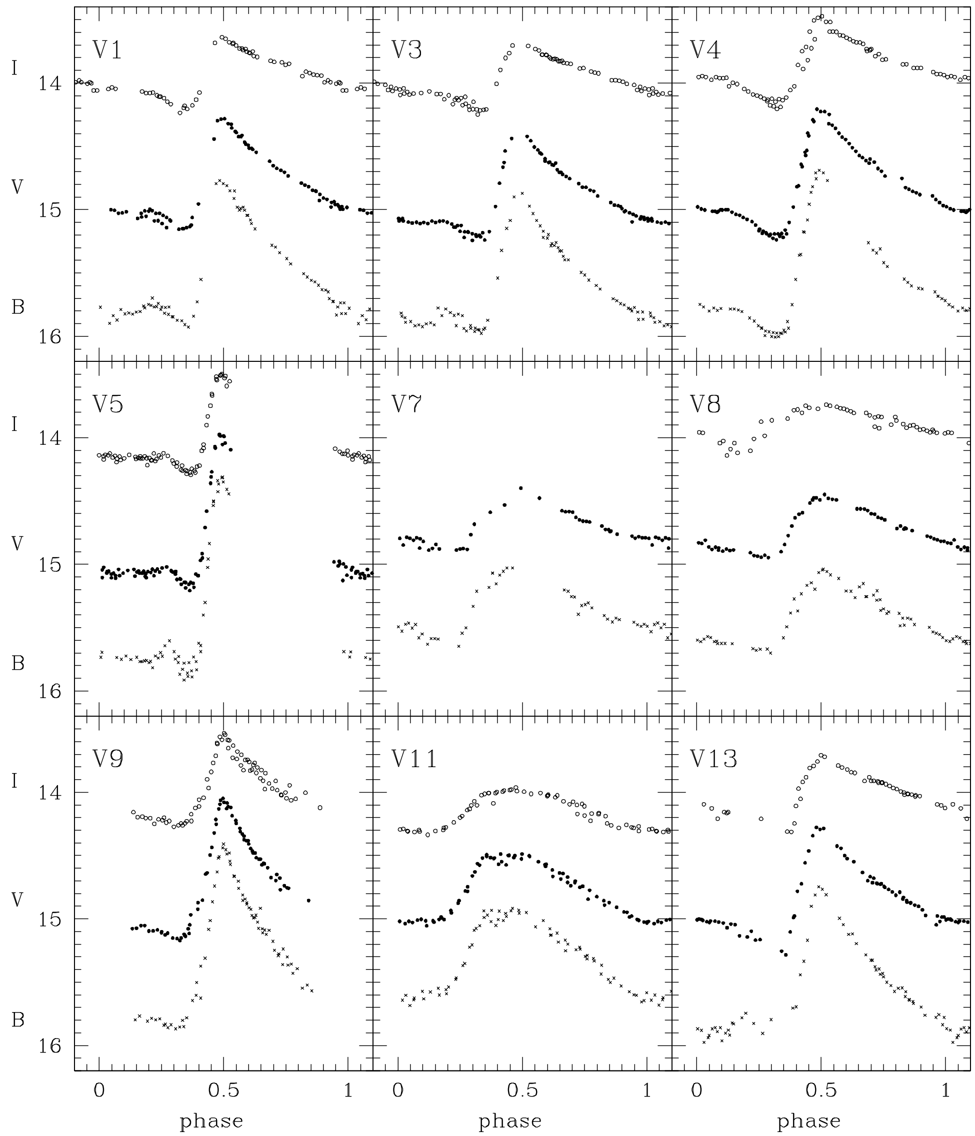

FIG. 3.—*B* (*stars*), *V* (*filled circles*), and *I* (*open circles*) light curves vs. the pulsational phase for RR Lyrae stars in NGC 3201. The pulsational phase was shifted in such a way that the phase of maximum light is equal to 0.5. Variable identifications are labeled.

4.1. *Amplitude Modulation*

During the last few years several empirical (Kovacs 1995; Nagy 1998; Bragaglia et al. 2000; Smith et al. 1999) and theoretical (Shibahashi 2000; van Hoolst 2000) investigations have been focused on amplitude modulation among field RR Lyrae stars. In a series of papers Szeidl (1976, 1988, and references therein) showed that approximately one-third of RR Lyrae stars show periodic or quasiperiodic variations in the luminosity amplitude. The timescale of the secondary modulation typically ranges from 11 days (AH Cam, Smith et al. 1994) to 530 days (RS Boo, Nagy 1998). The occurrence of this phenomenon, called the Blazhko effect (Blazhko 1907), among RR Lyrae variables in GGCs (M3, M5, M15, ω Cen) and in dwarf galaxies (Draco) was soundly confirmed by Smith (1981), who also found a similar frequency, i.e., 25%–30%. In this context it is worth mentioning that Corwin & Carney (2001) recently provided very accurate *BV* CCD photometry for more than 200 RR Lyrae stars in M3. The previous authors collected time-series data over a time interval of 5 yr, and therefore they unambiguously identified RR Lyrae variables that present amplitude modulations. The new data confirm the finding obtained by Smith, and indeed 47 out of 158 RR*ab* variables present the Blazhko effect, i.e., 30% of the sample. Moreover, a recent detailed Fourier analysis based on the MACHO database does suggest that some fundamental Blazhko RR Lyrae stars present both amplitude and phase modulation, as well as the occurrence of the Blazhko effect among first-overtone RR Lyrae stars (Kurtz et al. 2000).

As a consequence, we decided to investigate the occurrence of such a phenomenon in our RR Lyrae sample. Figure 6 shows the difference in the luminosity amplitude between current estimates and the luminosity amplitudes provided by C84. Data plotted in this figure disclose several interesting features: (1) a fraction of 25%–30% among fundamental variables present amplitude modulations; (2) one (V48) out of the three RR*c* variables in our sample shows amplitude modulation. This variable is the first candidate Blazhko RR*c* star in a GGC. The plausibility of these find-

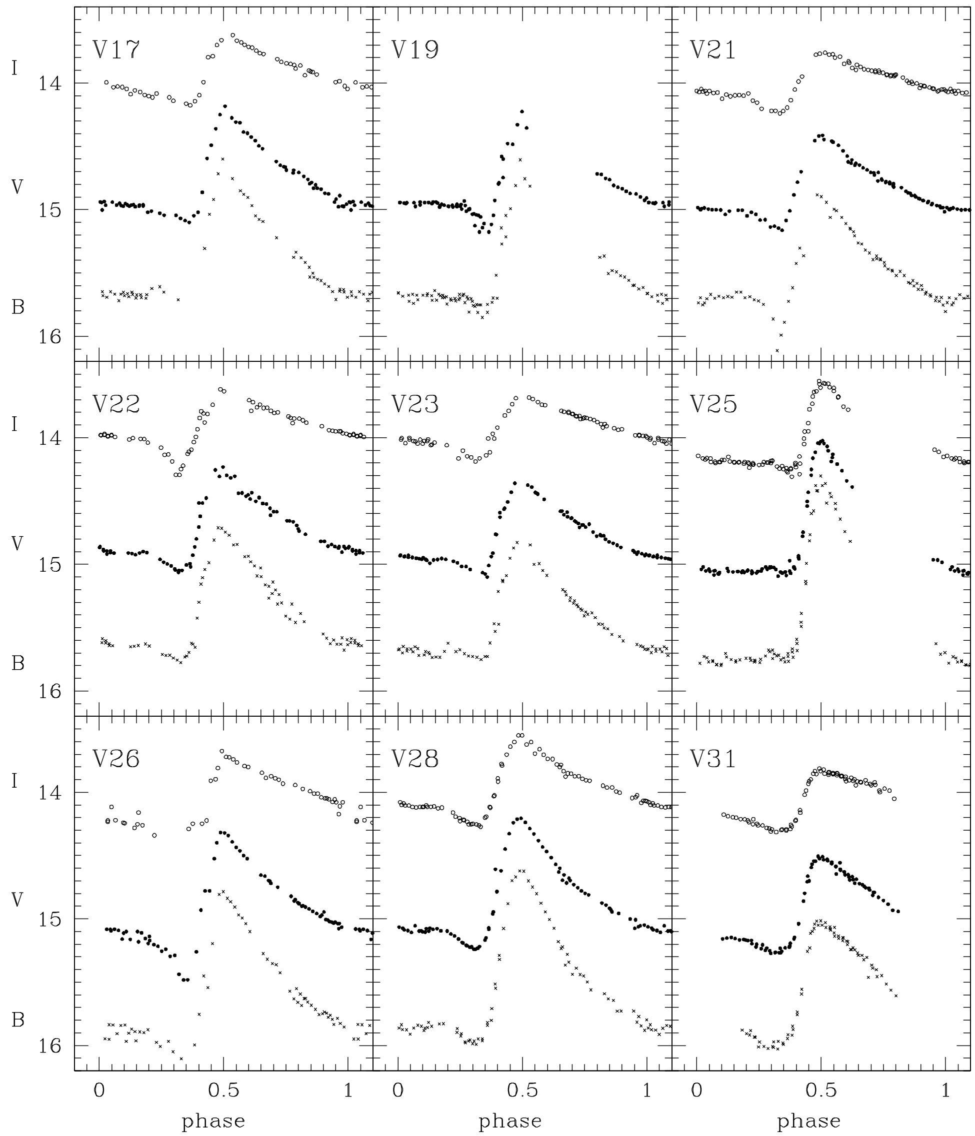

Fig. 3.—*Continued*

ings rely on the fact that all the RR Lyrae stars with amplitude modulations in the *B* band also show the modulation in the *V* band. Note that as a conservative estimate of the systematic difference between current photometry and the photographic photometry performed by C84, we only selected variables that show a difference in the luminosity amplitude larger than 0.1 and 0.15 mag in the *V* and in the *B*, respectively (*dashed lines*). The referee suggested that we compare current mean magnitudes with the mean magnitudes provided by C84 to single out whether some of the candidate Blazhko RR Lyrae stars are blends in one of the two data sets. Interestingly enough, we found that the mean *V* magnitudes provided by C84 for variables V31 and V36 are ≈0.12 and ≈0.20 mag brighter than current ones (see the Appendix for more details). This means that they could be blends in the former photometry. Oddly enough, the current mean *V* magnitude of variable V58 is 0.15 mag brighter than the mean magnitudes provided by C84. The reason for this discrepancy is not clear.

On the basis of this finding, we decided to extend our analysis by covering a longer baseline, and, in particular, to compare current *B* amplitudes with the *B* amplitudes estimated by SH73.

Figure 7 shows the difference between current and SH73 mean *B* magnitudes.[8] Data plotted in this figure display that mean *B* magnitudes by SH73 are systematically brighter and the difference ranges from a few hundredths up to ≈0.4 mag. According to this evidence we will consider as candidate Blazhko RR Lyrae stars those objects that present a difference between current and SH73 *B* amplitudes that is larger than 0.45 mag. The top panel of Figure 8 shows that approximately 30% of RR Lyrae variables present amplitude modulations larger than 0.45 mag. The same result applies to V48 (RR*c* variable). It is noteworthy that data plotted in Figure 8 seem to suggest that the difference in the *B* amplitude is mainly due to a difference in $B_{\rm min}$ (*middle*)

[8] Note that SH73 did not supply the mean *B* magnitudes, therefore to estimate the difference we adopted the mean between minimum and maximum.

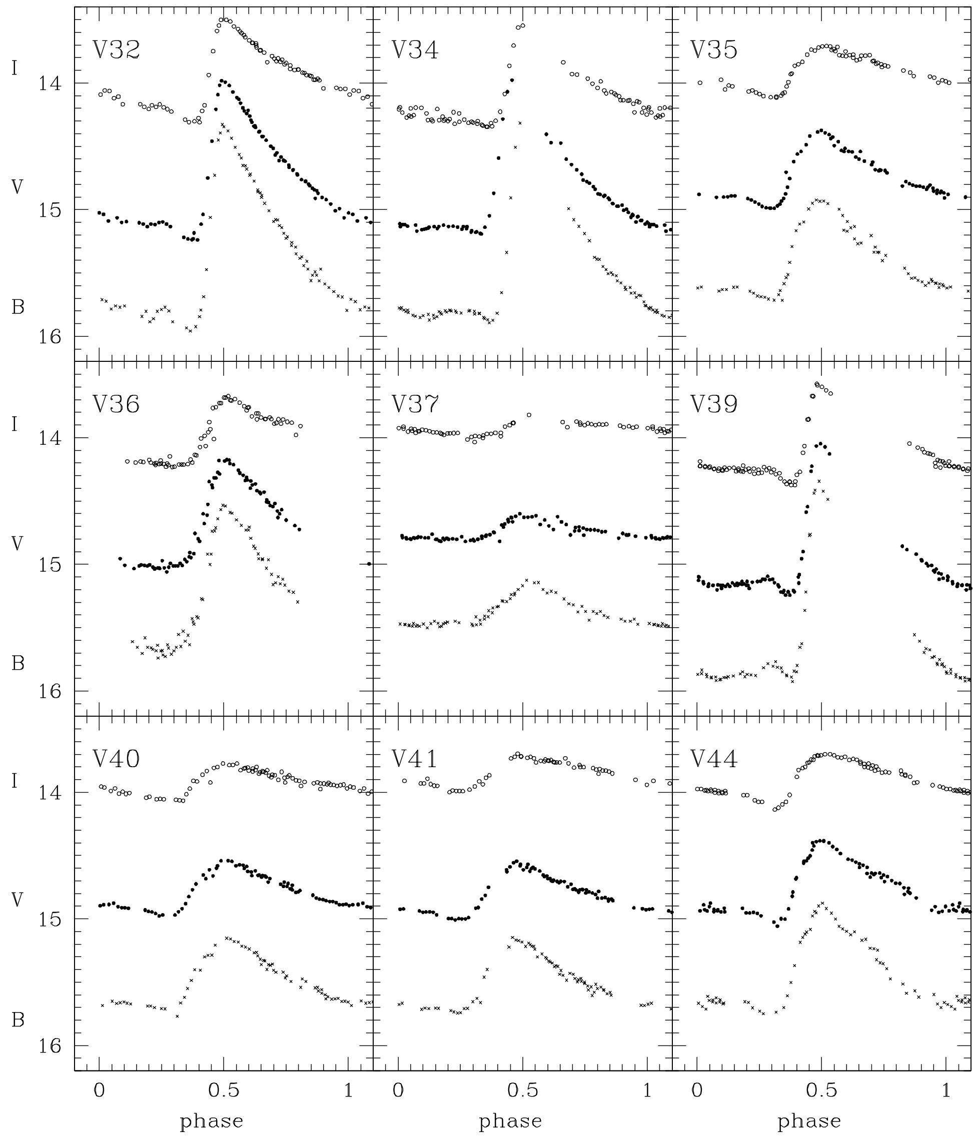

FIG. 3.—*Continued*

rather than in B_{max} (*bottom*). The systematic difference in the two data sets does not allow us to constrain this effect on a more quantitative basis.

We also note that approximately 50% of RR Lyrae stars that show amplitude modulation in the SH73 sample have also been detected in the C84 sample, namely V6, V26, V34, V48, and V51. As a whole, the comparison of photometric data spanning a time interval of roughly 25 yr strongly support the evidence that a fraction of 25%–30% of RR Lyrae stars in NGC 3201 present amplitude modulation (the Blazhko effect). Unfortunately, current data do not allow us to assess on a quantitative basis the secondary period. A comprehensive analysis based on new data as well as on old photographic data will be presented in a forthcoming paper (Bono et al. 2002).

In this context we also mention that the comparison between predicted and empirical amplitudes among cluster variables should be handled with caution. In fact, data plotted in Figure 9 clearly show that in the Bailey diagram both distribution and intrinsic scatter are somehow affected by the number of RR Lyrae stars that show the Blazhko effect. Note that current variations in the luminosity amplitude are indeed a lower limit to the "true" amplitude modulation. As a matter of fact, extensive data for field and cluster (M3) RR Lyrae stars do suggest that the luminosity variation is, on average, of the order of a half magnitude (see Fig. 3 in Szeidl 1988).

Table 1 lists, from left to right for each variable in our sample: column (1) the variable name, (2) the RR Lyrae type, (3) the period, (4) the reference for the period. Moreover, from columns (5) to (7) we give the magnitude-weighted *BVI* mean magnitudes, while from columns (8) to (10) the intensity-weighted *BVI* mean magnitudes. The last three columns ([11] to [13]) list the *BVI* luminosity amplitudes. The mean *I* magnitudes of RR Lyrae stars with noisy light curves have not been included. However, a photometric scatter slightly larger than the typical value (0.01–0.02 mag) can also be found among *BV* light curves of variables located close to the edges of the CCD camera.

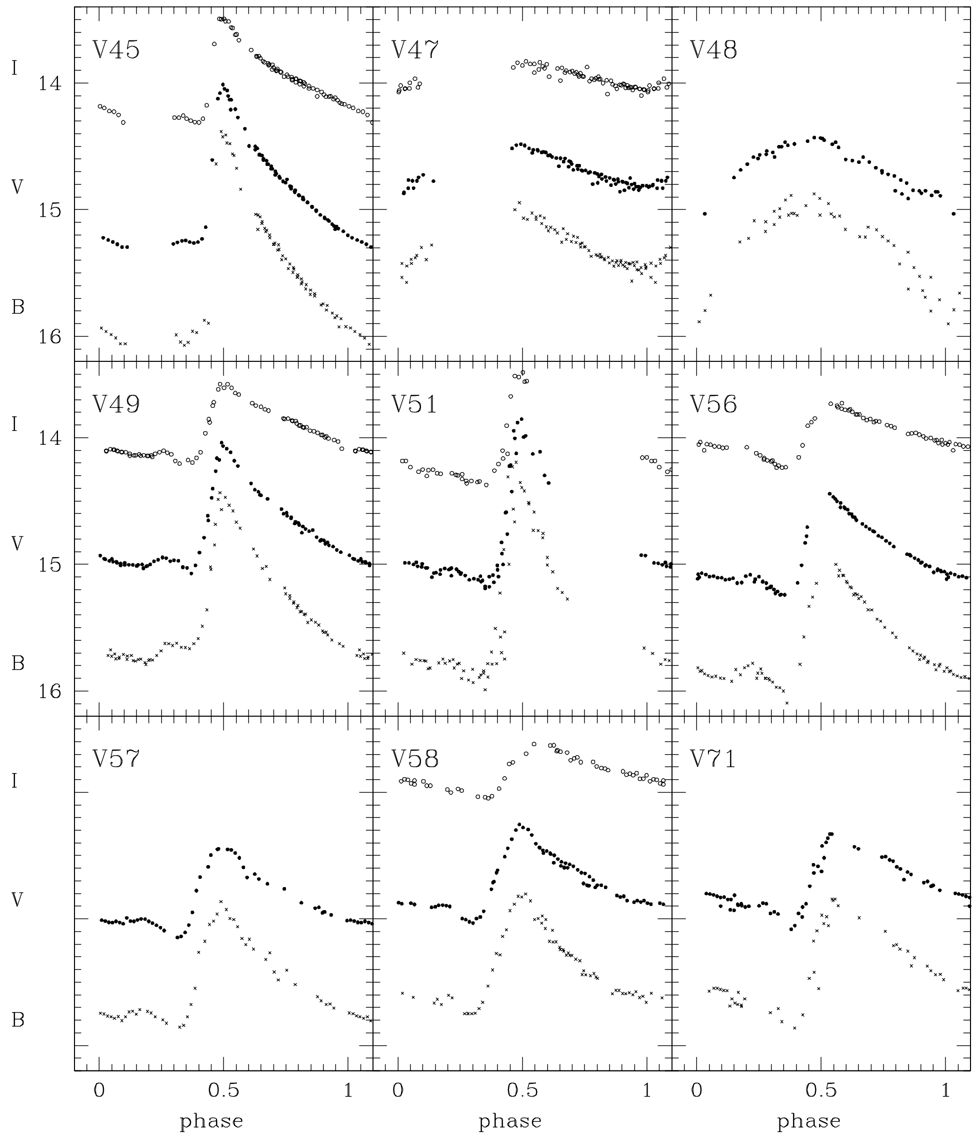

FIG. 3.—*Continued*

5. REDDENING EVALUATIONS

5.1. *RR Lyrae B−V Colors*

Accurate evaluations of the reddening across the central region of NGC 3201 are mandatory to supply robust estimates of intrinsic mean magnitudes and colors of RR Lyrae stars. However, precise reddening estimates are difficult, and the problem for NGC 3201 is even more complicated since this cluster presents patchy absorptions, i.e., differential reddening, across the main body of the cluster (Zinn 1980; Alcaino & Liller 1981; Da Costa et al. 1981; C84; CO97; Layden et al. 2002, hereafter L02). As a matter of fact, current color excess estimates range from $E(B-V) = 0.21$ to $E(B-V) = 0.29$ according to mean RR Lyrae colors (C84). On the basis of spectroscopic data for a sizable sample of red giants GW98 found $E(B-V)$ values ranging from 0.21 to 0.31. The same result applies to mean reddening values, and indeed current values present a spread ranging from 0.21 ± 0.03 (C84), 0.22 ± 0.03 (CO97) to 0.28 (Harris 1976).

A comprehensive analysis of the extinction map across NGC 3201 has been recently provided by vBM01 based on high-quality and deep *V*- and *I*-band data. In particular, they found a differential reddening of the order of 0.2 mag and a reasonable agreement on a large scale with the dust infrared maps provided by Schlegel, Finkbeiner, & Davis (1998, hereafter SFD98). At the same time they confirmed the evidence originally brought out by Arce & Goodman (1999) that infrared emissions maps overestimate reddening in high extinction regions [$E(B-V) > 0.15$]. However, the zero point of the reddening scale found by vBM01 [$E(V-I) = 0.15$] is approximately 1.5 σ smaller than mean values available in the literature. As a consequence, we decided to estimate the mean value of the color excess, as well as of its variation across the cluster, using the pulsation properties of our RR Lyrae sample.

In their seminal investigations Preston (1964) and Sturch (1966) calibrated an empirical relation for RR*ab* variables that supplies the color excess $E(B-V)$ as a function of the $B-V$ color at the phase of luminosity minimum, the period,

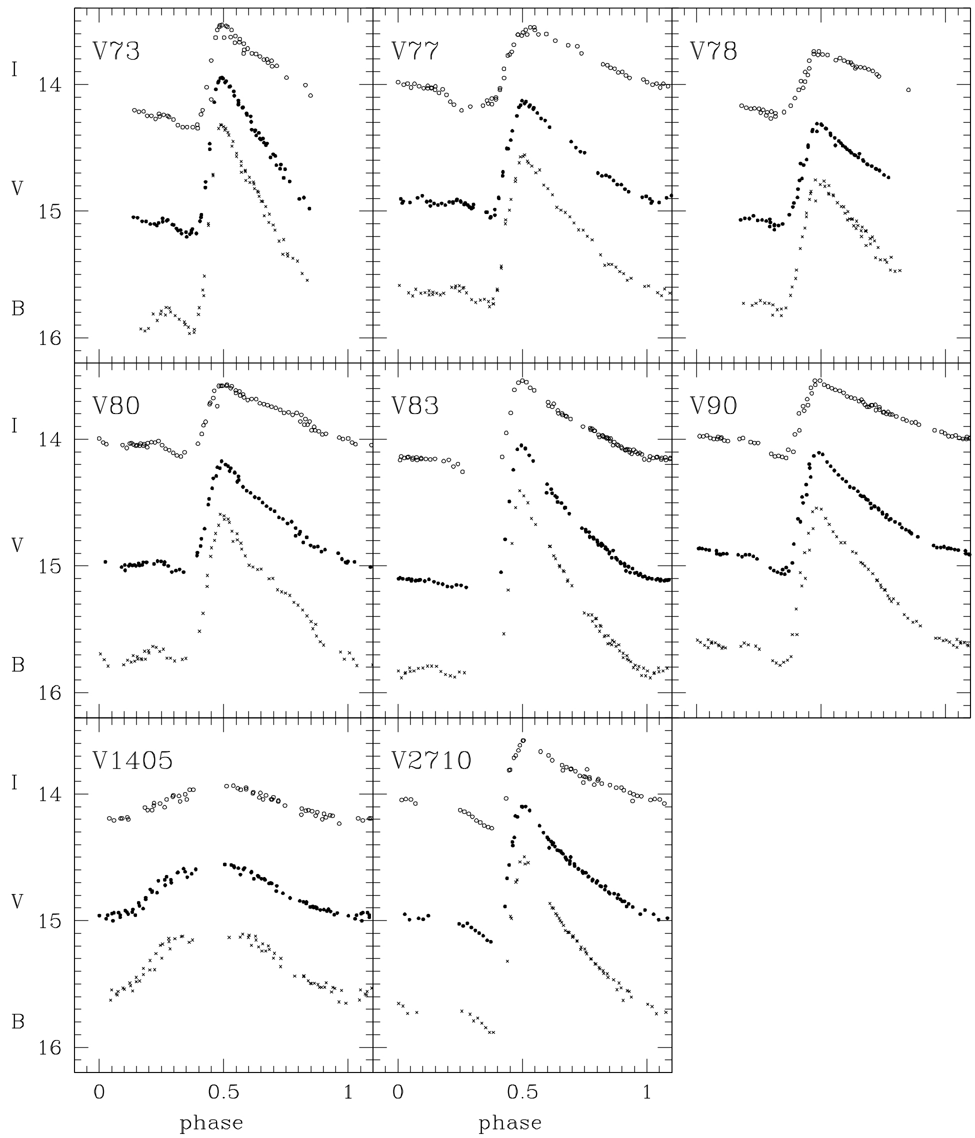

FIG. 3.—*Continued*

and the metallicity. Following Walker (1990, hereafter W90), who improved this empirical relation, we adopt $E(B-V) = (B-V)_{\rm min} - 0.24P - 0.056[{\rm Fe/H}] - 0.336$, where $(B-V)_{\rm min}$ is the mean color over the pulsation phases $0.5 \leq \phi \leq 0.8$, [Fe/H] is the metal content in the ZW84 metallicity scale, and P the fundamental period (days). On the basis of $(B-V)_{\rm min}$ colors listed in column (3) of Table 2 and by adopting the cluster iron abundance given by ZW84, $[{\rm Fe/H}] = -1.61$, we found that the mean value of the reddening is $\langle E(B-V)\rangle = 0.34 \pm 0.03$ and the individual values (col. [4] in Table 2) range from 0.29 (V36) to 0.40 (V13). Individual estimates do suggest that across the cluster region covered by RR Lyrae stars in our sample the reddening changes by approximately 0.1 mag. This finding supports the results obtained by GW98 on the basis of spectroscopic measurements of 17 cluster RGs. On the other hand, the mean value estimated over the entire sample as a weighted mean should be cautiously treated. In fact, empirical evidence does suggest that reddening evaluations based on the Sturch's method are typically 0.03 mag larger than the determinations based on the slope of the RGB in the (V, $V-I$) CMD (Walker & Nemec 1996).

Therefore, we decided to provide new empirical evaluations of intrinsic $B-V$ and $V-I$ RR Lyrae colors by adopting two different routes. Since Schwarzschild (1940) it is well known that RR Lyrae stars obey to a period-color (PC) relation. This evidence was further strengthened by empirical and theoretical investigations (Sandage et al. 1990a; Caputo & De Santis 1992; Fernley 1993). At the same time theoretical predictions based on nonlinear, convective models suggest that the luminosity amplitude is strongly correlated with the effective temperature and presents a negligible dependence on stellar mass and metallicity (Bono et al. 1997c). To derive robust empirical PC relations and amplitude-color (AC) relations we selected two GGCs, namely, M5 and IC 4499. These clusters present a sizable sample of RR Lyrae stars, have a metallicity similar to NGC 3201, and are not affected by differential reddening. According to the ZW84 metallicity scale the metallicity of these clusters is $[{\rm Fe/H}] = -1.5$ (M5) and $[{\rm Fe/H}] = -1.4$ (IC 4499). Pulsa-

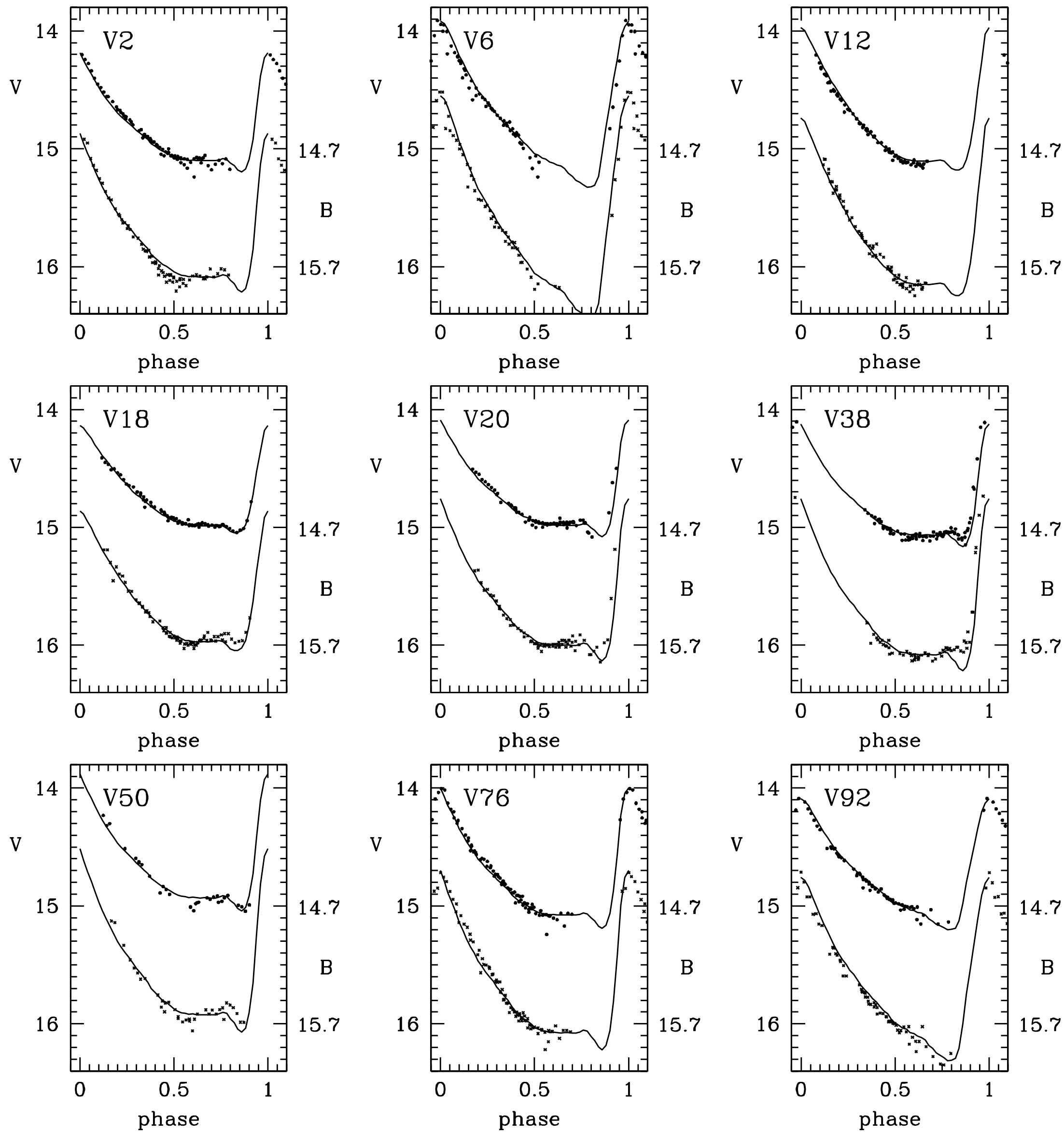

FIG. 4.—*B* and *V* light curves of RR*ab* variables with periods close to 0.5 days and poor phase coverage close to the phase of minimum and/or maximum light. The solid lines display the Layden's template adopted to fit empirical data. See text for further details.

tion properties for RR Lyrae stars in M5 were taken from Brocato, Castellani, & Ripepi (1996), Caputo at al. (1998), Storm, Carney, & Beck (1991), and Reid (1996), while for RR Lyrae stars in IC 4499 they are from Walker & Nemec (1996).

However, the attempt to derive intrinsic colors with either the PC or the AC relation was unsuccessful. In fact, the $B-V$ and the $V-I$ residuals clearly show a trend either with the luminosity amplitude or the mean color, respectively. The reason the empirical relations do not work is not clear. The failure of the PC relation in the optical bands might be due to the intrinsic width of the fundamental instability strip, as well as to the dependence on the metal abundance that causes an increase in the color scatter at fixed periods. The AC relation might be affected by the same drawback as well as by the scatter introduced by RR Lyrae stars affected by amplitude modulation. To overcome this thorny problem, we decided to derive, according to Caputo & De Santis (1992, hereafter CDS92), an empirical relation connecting the intrinsic color of RR Lyrae stars to the luminosity amplitude in the *B* band and to the metallicity. To cover a wide metallicity range, we selected field RR Lyrae stars observed by Lub (1977) and by Carney et al. (1992a). As far as the Lub sample is concerned, we adopted the pulsation parameters collected by Sandage (1990b). Objects that present amplitude modulations have been neglected. We ended up with a sample of 78 RR Lyrae stars whose metallicity ranges from [Fe/H] $= -2.2$ to [Fe/H] $= 0$. We found that these objects do obey to a well-defined amplitude-color-metallicity (ACZ) relation:

$$(B-V)_0 = 0.448(\pm 0.017) - 0.078(\pm 0.006)A_B + 0.012(\pm 0.004)[Fe/H]\ \sigma = 0.016\ ,$$

where the symbols have their usual meaning and units. Both the constant term and the coefficient of the luminosity amplitude are quite similar to the values found by CDS92 (see their relation 10). On the other hand, the coefficient of

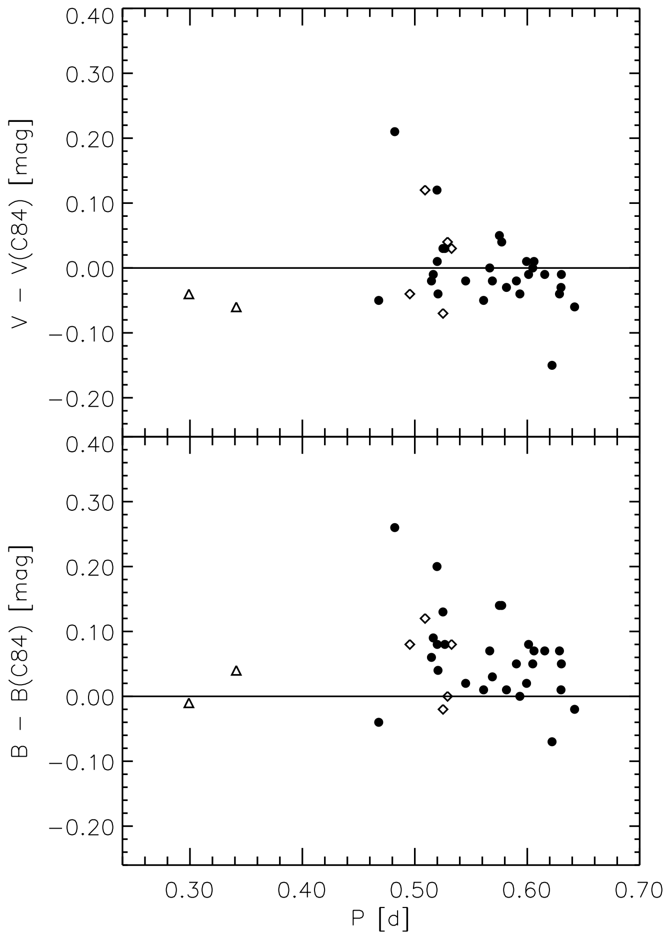

FIG. 5.—Difference in the mean $\langle V \rangle$ (*top*) and $\langle B \rangle$ (*bottom*) magnitude for variables in common with C84. Triangles show first overtones, while circles RR*ab* stars. Diamonds display fundamental variables with poor phase coverage.

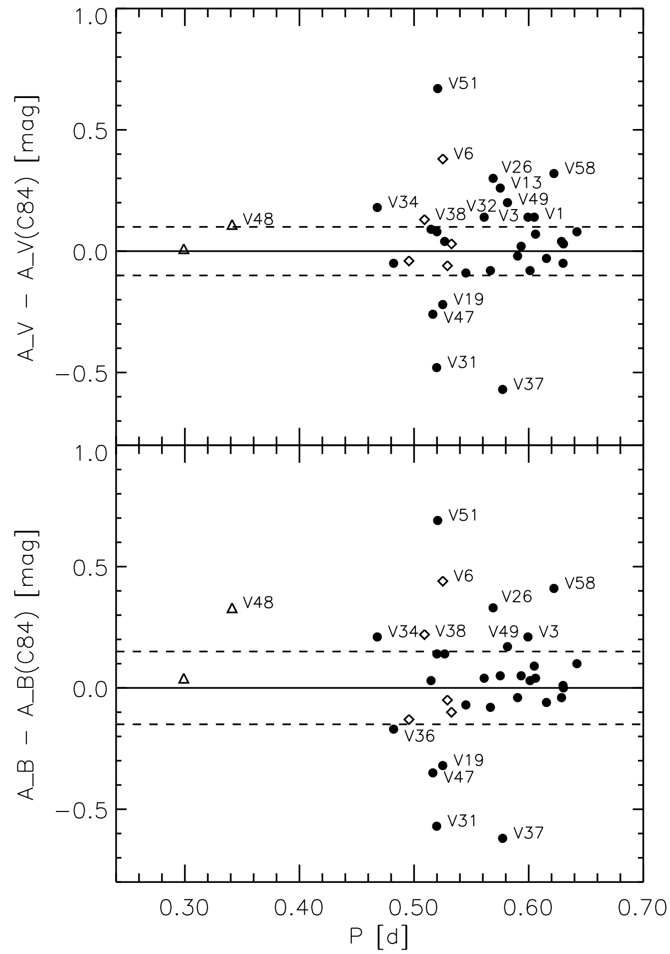

FIG. 6.—Difference in the V (*top*) and in the B (*bottom*) amplitude vs. period for variables in common with C84. Variables that show amplitude variations larger than 0.10 mag in the V band and of 0.15 mag in the B band (*dashed lines*) have been labeled. The symbols are the same as in Fig. 5.

the metallicity term is almost a factor of two larger (0.012 vs. 0.006) in the current relation than in the CDS92's relation. The difference seems to be due to the increase in the sample size and to the inclusion of metal-rich RR Lyrae stars (Carney et al. 1992a).

To check whether the current relation could be further improved, we correlated the intrinsic mean $B-V$ color to period, luminosity amplitude, and metallicity. The linear regression over the same RR Lyrae sample supplies the following period-amplitude-color-metallicity (PACZ) relation:

$$\begin{aligned}(B-V)_0 = {} & 0.507(\pm 0.014) - 0.052(\pm 0.007)A_B \\ & + 0.223(\pm 0.039)\log P \\ & + 0.036(\pm 0.005)[Fe/H]\ \sigma = 0.014 \ .\end{aligned}$$

Note that such a relation relies on the assumption that the current sample of RR Lyrae stars is representative of the entire population. To validate the accuracy of these relations based on field RR Lyrae stars, we applied it to RR Lyrae stars in M3, since this cluster is only marginally affected by reddening [$E(B-V) \approx 0.01$, Dutra & Bica 2000, hereafter DB00]. We selected, among the RR Lyrae variables (207) observed by Corwin & Carney (2001) in M3, the fundamental ones that are not affected by blends and present accurate estimates of both periods and B amplitudes. We ended up with a sample of 127 RR Lyrae stars. By assuming a metal content for M3 of [Fe/H] $= -1.46$ (Kraft et al. 1995) and by applying the ACZ relation to this subsample, we found a mean cluster reddening of $\langle E(B-V) \rangle = 0.008 \pm 0.027$, while by adopting the PACZ relation we found $\langle E(B-V) \rangle = 0.007 \pm 0.024$. To avoid any spurious effect, if any, introduced by RR Lyrae stars that present the Blazhko effect, we only selected "canonical" RR Lyrae stars (81). On the basis of the new sample the ACZ and the PACZ relation give $\langle E(B-V) \rangle = 0.012 \pm 0.027$ and $\langle E(B-V) \rangle = 0.011 \pm 0.024$, respectively. The difference in the mean cluster reddenings based on the two different samples is negligible as a result of the marginal dependency of mean colors on amplitude modulations (*crosses*, Fig. 10). The previous estimates are, within the errors, in very good agreement with the values given in the literature. The difference between ACZ and PACZ relation is negligible. However, color estimates based on the latter one present a slightly smaller intrinsic scatter.

As a further independent test we applied the previous relation to fundamental RR Lyrae stars not affected by amplitude modulation in several GGCs. We found that the mean reddenings as well as the dispersions are, within the uncertainties, in very good agreement (see data listed in col. [5] of Table 3) with similar estimates available in the litera-

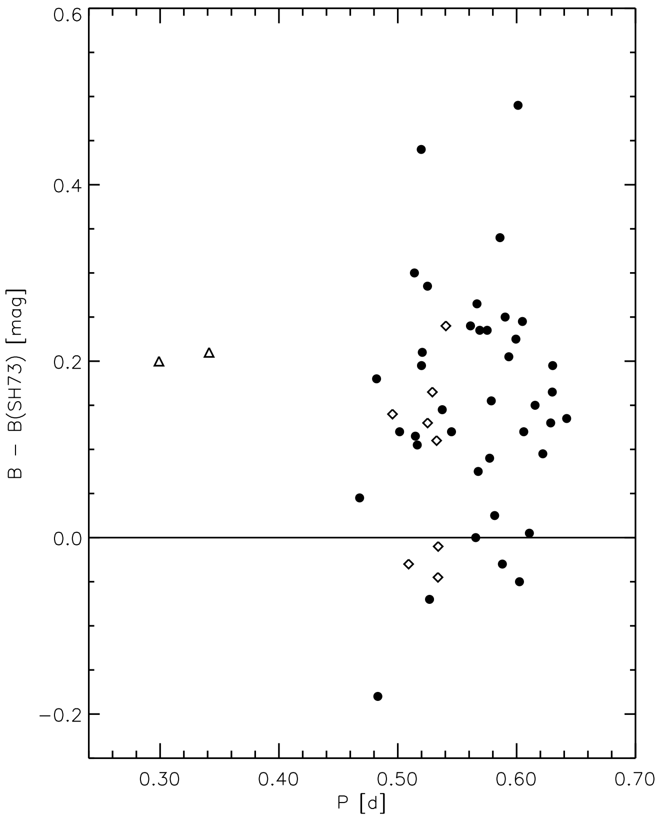

FIG. 7.—Difference in the mean $\langle B \rangle$ magnitude $[\langle B \rangle = (B_{\max} + B_{\min}) \times 0.5]$ for variables in common with SH73.

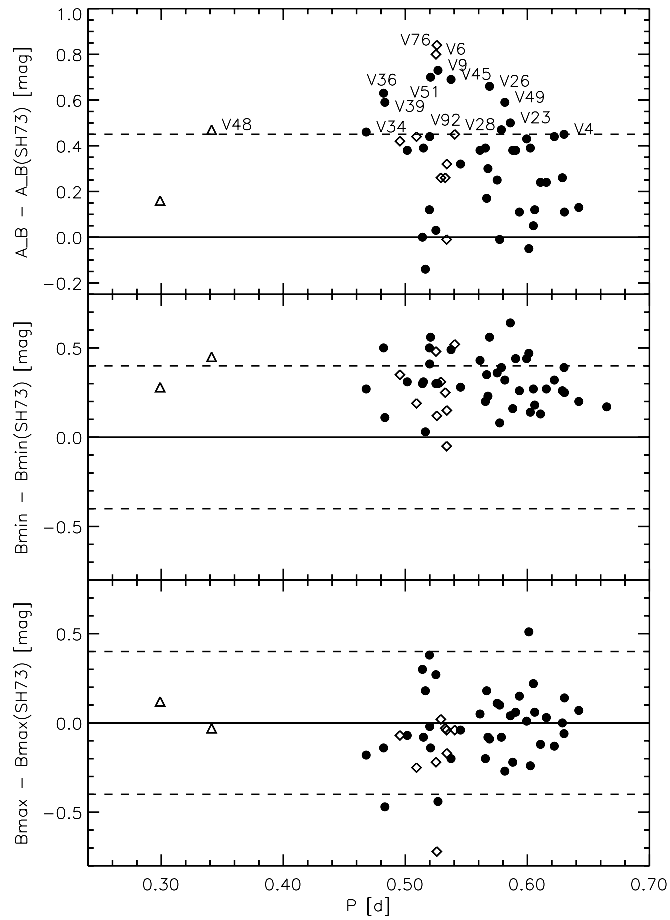

FIG. 8.—*Top*: Difference in the *B* amplitude vs. the pulsation period for variables in common with SH73. Variables that show amplitude variations larger than 0.45 mag have been labeled. The symbols are the same as in Fig. 5. *Middle*: Same as top, but the difference is referred to the minimum in luminosity. *Bottom*: Same as middle, but for the maximum in luminosity.

ture and based on stellar colors or on far-infrared dust emission (SFD98; DB00). On the basis of this evidence we estimated the individual reddenings and, in turn, the intrinsic $B-V$ colors of RR Lyrae stars in our sample (see data listed in cols. [5] and [6] of Table 2). We found that the mean reddening is $\langle E(B-V) \rangle = 0.30 \pm 0.03$ if we assume $[\mathrm{Fe/H}] = -1.42$, while the single values range from 0.22 (V36) to 0.35 (V45). Note that individual reddening estimates based on $B-V$ colors are typically affected by an uncertainty of the order of 0.03 mag. The error budget includes the uncertainty affecting the photometric calibration ($\sigma_{B,V} \approx 0.02$ mag), the intrinsic scatter of the PACZ relation (± 0.01 mag), as well as the error on the assumption that the reddening toward M3 is $E(B-V) = 0.01$. We did not account for the uncertainty in the mean metallicity, and indeed the mean reddening ranges from $\langle E(B-V) \rangle = 0.29 \pm 0.03$ to $\langle E(B-V) \rangle = 0.31 \pm 0.03$ if we assume $[\mathrm{Fe/H}] = -1.23$ (CG97) or $[\mathrm{Fe/H}] = -1.61$ (ZW84). Current mean reddening values, if we account for the entire error budget, support the mean reddening value obtained by adopting the SFD98 map. In fact, the mean reddening provided by this map over the same cluster region covered by our RR Lyrae sample is $\langle E(B-V) \rangle \approx 0.26 \pm 0.02$. This finding supports the absolute zero point of the SFD98 map.

5.2. *RR Lyrae V−I Colors*

We collected photometric data in three different bands, and therefore we can constrain the occurrence of systematic errors, if any, in the reddening evaluations based on $B-V$ colors. To estimate the intrinsic $V-I$ colors, we selected among field RR Lyrae stars the objects, as for $B-V$ colors, for which accurate estimates of $V-I$ color, metallicity, and reddening are available. We ended up with a sample of 18 RR*ab* stars (see Table 4). However, we realized that this sample is affected by a selection bias. In fact, all of them were originally chosen to perform the Baade-Wesselink analysis, and therefore they present large luminosity amplitudes and are typically located close to the blue edge. As a consequence, we decided to include two GGCs that host a sizable sample of RR Lyrae stars and accurate V and I photometry, namely, IC 4499 (Walker & Nemec 1996, $N_{\mathrm{RR}} = 35$) and NGC 6362 (A. Walker 2001, private communication, $N_{\mathrm{RR}} = 14$). On the basis of these data we found that they do obey to the following period-amplitude-color (PAC) relation:

$$(V-I)_0 = 0.65(\pm 0.02) - 0.07(\pm 0.01) A_V + 0.36(\pm 0.06) \log P \;\; \sigma = 0.02 \; ,$$

where the symbols have their usual meaning. This relation, when compared with the previous one, presents a key difference: the coefficient of the metallicity term is vanishing, and therefore the linear regression was performed by neglecting this parameter. This effect is due to the fact that the $V-I$ colors present a mild dependence on metallicity. However,

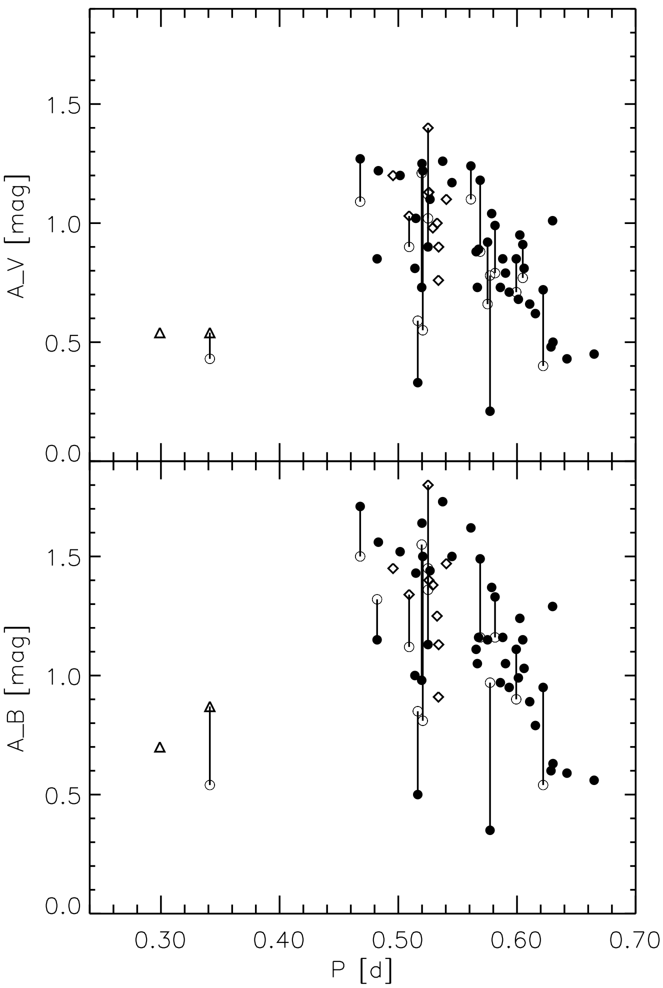

FIG. 9.—Bailey diagram for RR Lyrae stars in our sample. Symbols are the same as in Fig. 5. Solid lines connect current amplitudes with the amplitudes estimated by C84 (*open circles*) for variables that show variations larger than 0.10 mag in the V (*top*) and of 0.15 mag in the B (*bottom*) band.

we cannot firmly assess whether this is an intrinsic behavior of RR Lyrae stars. In fact, RR Lyrae stars listed in Table 4, together with RR Lyrae stars in IC 4499 and NGC 6362, cover a wide metallicity range, but only one object is more metal-poor than [Fe/H] $= -1.7$.

To estimate the accuracy of this relation, it was applied to cluster RR Lyrae stars for which homogeneous estimates of mean $B-V$ and $V-I$ colors are available. Column (6) of Table 3 gives the mean reddening values and the standard deviations. As a whole, we found that reddening estimates based on $V-I$ intrinsic colors are in good agreement with those based on $B-V$ colors, and indeed the $\langle E(V-I)\rangle$ values are, within the errors, approximately equal to $1.22 \times \langle E(B-V)\rangle$ (Cardelli, Clayton, & Mathis 1989; Bessell 1979). However, the mean reddening of NGC 1851 based on $V-I$ colors is smaller than the reddening based on $B-V$ colors. It has been recently claimed (Kovacs & Walker 2001, hereafter KW01) that the zero point of the I-band photometry of this cluster could be affected by a systematic error. This, notwithstanding the agreement between the two independent reddening estimates, strengthens the plausibility and the accuracy of previous PACZ and PAC relations. Any further analysis concerning the difference between the two reddening scales is premature. In fact, the accuracy of the absolute zero point of the PAC relations was not checked with a template cluster such as M3, since current I-band data could still be affected by uncertainties in the absolute zero-point calibration (Ferraro et al. 1997).

However, individual reddening estimates, based on the PAC relation listed in Table 5, are in very good agreement with the evaluations based on the PACZ relation, and indeed the bulk of them attain values roughly equal to $1.22 \times \langle E(B-V)\rangle$. Moreover, we find that the mean reddening is $\langle E(V-I)\rangle = 0.36 \pm 0.05$, while the single values range from 0.28 (V36) to 0.45 (V45). Note that the reddenings based on $V-I$ colors are affected by an uncertainty of the order of 0.04 mag. The error budget includes the error on the photometric calibration ($\sigma_I \approx 0.03$) and on the intrinsic scatter of the PAC relation ($\sigma_I \approx 0.02$). This notwithstanding, current results strongly support the finding obtained by vBM01 on the basis of TO star colors. In fact, we find that, across the cluster, the $E(V-I)$ values undergo differential changes up to $\sim$0.17 mag. This differential variation agrees quite well with the reddening estimates by vBM01, and indeed across the same cluster region (see their Fig. 4) their reddening estimates [$E(V-I)$] range from 0.18 to 0.35, respectively. On the other hand, our estimates do suggest a zero point larger than that evaluated by vBM01. As a matter of fact, we find that the mean reddening in the cluster region covered by our observations is $\langle E(V-I)\rangle = 0.36 \pm 0.05$, while the mean reddening based on the vBM01 map supplies $\langle E(V-I)\rangle = 0.25 \pm 0.07$. The reasons for this difference are not clear. A plausible reason could be the effect of heterochromatic extinction between TO and HB stars (Roberts & Grebel 1995; Anthony-Twarog & Twarog 2000). Note that the current reddening estimate agrees, within the errors, with the mean reddening obtained using the SFD98 map, and indeed we find $\langle E(V-I)\rangle = 1.22 \times \langle E(B-V)\rangle = 0.32 \pm 0.02$.

To constrain once again the intrinsic accuracy of current reddening estimates, we decided to perform a new test. According to a well-established result the minimum-light color of RR*ab* stars present a mild dependence on metallicity (Lub 1979). This evidence has been further strengthened by Mateo et al. (1995, hereafter M95) who found that the mean minimum-light $V-I$ colors of a dozen of well-observed field RR Lyrae stars is roughly equal to 0.58 ± 0.03 mag. We estimated once again the individual reddenings (col. [5] in Table 5), and, interestingly enough, the new estimates are in good agreement with reddening evaluations based on the PAC relation. As a matter of fact, we found $\langle E(V-I)\rangle = 0.36 \pm 0.05$, while individual reddenings range from 0.24 (V36) to 0.46 (V4).

5.3. *Fourier Coefficients*

During the last few years several investigations have been devoted to the Fourier analysis of empirical light curves of RR Lyrae variables (Kovacs & Kanbur 1998). The underlying idea of these studies is to derive empirical relations based on Fourier coefficients that can be safely adopted to estimate physical parameters, such as absolute magnitude, intrinsic color, and metallicity of variable stars (Simon & Clement 1992; Jurcsik & Kovacs 1996; KW01). Therefore we followed this approach to supply an independent estimate of individual RR Lyrae reddenings. At first we performed the fit of the V-band light curves by means of sine

TABLE 1

Pulsational Properties of RR Lyrae Stars in NGC 3201

ID[a] (1)	Type (2)	Period[b] (3)	Ref.[c] (4)	B_m[d] (5)	V_m[d] (6)	I_m[d] (7)	$\langle B \rangle$[e] (8)	$\langle V \rangle$[e] (9)	$\langle I \rangle$[e] (10)	$A(B)$[f] (11)	$A(V)$[f] (12)	$A(I)$[f] (13)
1	*ab*	0.6048761	SH73	15.51	14.83	13.95	15.45	14.79	13.94	1.15	0.91	0.57
2[g]	*ab*	0.5326722	C84	15.47	14.87	...	15.35	14.82	...	1.25	1.00	...
3[h]	*ab*	0.5993792	C84	15.60	14.90	13.97	15.54	14.87	13.96	1.11	0.85	0.56
4	*ab*	0.6300096	C84	15.50	14.81	13.87	15.43	14.77	13.86	1.29	1.02	0.69
5	*ab*	0.501536	SH73	15.38	14.78	13.99	15.27	14.71	13.97	1.52	1.20	0.78
6[g,h]	*ab*	0.5250936	C84	15.37	14.76	...	15.21	14.67	...	1.8	1.40	...
7	*ab*	0.6303322	SH73	15.33	14.68	...	15.31	14.67	...	0.63	0.50	...
8	*ab*	0.6286573	C84	15.42	14.72	13.90	15.41	14.71	13.89	0.60	0.48	0.35
9	*ab*	0.5267087	C84	15.45	14.81	14.03	15.36	14.76	14.02	1.45	1.10	0.71
11	*c*	0.2990490	C84	15.29	14.78	14.15	15.26	14.76	14.15	0.70	0.54	0.34
12[g]	*ab*	0.4955547	C84	15.44	14.78	...	15.33	14.71	...	1.45	1.2	...
13	*ab*	0.5752145	SH73	15.54	14.85	14.03	15.48	14.81	14.02	1.15	0.96	0.56
17	*ab*	0.5655773	SH73	15.39	14.77	13.93	15.34	14.74	13.92	1.11	0.88	0.54
18[g]	*ab*	0.5395	L02	15.35	14.74	...	15.29	14.70	...	1.13	0.9	...
19[h]	*ab*	0.5250201	SH73	15.42	14.76	...	15.36	14.74	...	1.13	0.90	...
20[g]	*ab*	0.5291045	C84	15.38	14.75	...	15.30	14.71	...	1.3	0.98	...
21	*ab*	0.5666280	C84	15.50	14.84	14.00	15.46	14.82	13.99	1.05	0.73	0.48
22	*ab*	0.6059882	C84	15.39	14.73	13.91	15.34	14.70	13.90	1.03	0.81	0.67
23	*ab*	0.586	PW	15.44	14.78	13.91	15.40	14.76	13.90	0.97	0.73	0.51
25	*ab*	0.5148010	C84	15.38	14.78	13.98	15.27	14.73	13.96	1.43	1.03	0.70
26[h]	*ab*	0.5689721	C84	15.63	14.93	14.07	15.55	14.89	14.05	1.53	1.18	0.62
28	*ab*	0.5786766	SH73	15.52	14.84	13.98	15.43	14.81	13.96	1.37	1.04	0.70
31[h]	*ab*	0.5197267	C84	15.60	14.95	14.04	15.56	14.93	14.03	0.98	0.73	0.47
32	*ab*	0.5611656	SH73	15.41	14.80	13.92	15.29	14.72	13.90	1.62	1.24	0.80
34[h]	*ab*	0.4678900	C84	15.37	14.80	14.03	15.21	14.75	14.00	1.71	1.27	0.84
35	*ab*	0.6155244	C84	15.42	14.74	13.87	15.38	14.73	13.86	0.79	0.62	0.40
36	*ab*	0.482143	PW	15.29	14.74	13.98	15.23	14.71	13.97	1.15	0.85	0.53
37[h]	*ab*	0.5772897	C84	15.37	14.74	13.92	15.37	14.74	13.92	0.35	0.21	0.16
38[g,h]	*ab*	0.5091250	C84	15.44	14.82	...	15.35	14.78	...	1.38	1.03	...
39	*ab*	0.4832092	SH73	15.47	14.85	14.04	15.36	14.79	14.01	1.56	1.22	0.77
40	*ab*	0.6421096	C84	15.50	14.79	13.91	15.48	14.78	13.91	0.59	0.43	0.29
41	*ab*	0.665	PW	15.52	14.82	13.85	15.50	14.81	13.85	0.56	0.45	0.28
44	*ab*	0.6107344	SH73	15.44	14.76	13.86	15.41	14.75	13.86	0.89	0.66	0.41
45	*ab*	0.5374165	SH73	15.61	14.94	14.03	15.48	14.87	14.01	1.73	1.26	0.83
47[h]	*ab*	0.5164	PW	15.23	14.67	13.95	15.22	14.66	13.95	0.50	0.33	0.20
48[h]	*c*	0.3412136	C84	15.27	14.68	...	15.24	14.67	...	0.87	0.54	...
49	*ab*	0.5815089	C84	15.37	14.73	13.93	15.29	14.69	13.91	1.33	0.99	0.64
50[g]	*ab*	0.5338	PW	15.26	14.66	...	15.16	14.60	...	1.45	1.15	...
51[h]	*ab*	0.5206220	C84	15.44	14.76	...	15.34	14.70	...	1.50	1.22	...
56	*ab*	0.5903376	C84	15.62	14.92	13.97	15.58	14.89	13.96	1.08	0.79	0.51
57	*ab*	0.5934337	C84	15.52	14.85	...	15.47	14.83	...	0.95	0.71	...
58[h]	*ab*	0.6220418	C84	15.42	14.73	13.85	15.39	14.70	13.84	0.95	0.72	0.43
71	*ab*	0.6011859	SH73	15.39	14.71	...	15.35	14.69	...	0.99	0.68	...
73	*ab*	0.5199500	SH73	15.45	14.80	13.98	15.32	14.73	13.96	1.64	1.25	0.83
76[g]	*ab*	0.52577	PW	15.42	14.80	...	15.32	14.75	...	1.42	1.13	...
77	*ab*	0.5676648	SH73	15.34	14.71	13.91	15.27	14.67	13.89	1.16	0.89	0.64
78	*ab*	0.514	SH73	15.45	14.82	14.02	15.39	14.79	14.01	1.00	0.81	0.50
80	*ab*	0.588	PW	15.40	14.76	13.87	15.34	14.73	13.85	1.16	0.85	0.56
83	*ab*	0.5451998	C84	15.46	14.84	13.95	15.36	14.78	13.93	1.50	1.17	0.79
90	*ab*	0.6024	PW	15.33	14.69	13.87	15.26	14.65	13.85	1.24	0.95	0.61
92[g]	*ab*	0.54047	PW	15.38	14.75	...	15.27	14.70	...	1.47	1.1	...
1405	*c*	0.3346	PW	15.33	14.76	14.04	15.31	14.75	14.04	0.51	0.40	0.27
2710	*ab*	0.548	PW	15.39	14.77	13.95	15.30	14.72	13.93	1.38	1.06	0.72

[a] Variable identification. The number is from Sawyer-Hogg 1973 except for the new variables for which the Lee's 1977 designation has been adopted.

[b] Pulsational period (days).

[c] References for period estimates (C84: Cacciari 1984; SH73: Sawyer-Hogg 1973; PW: present work; L02: Layden et al. 2002).

[d] Mean magnitude-weighted *B*, *V*, and *I* magnitudes.

[e] Mean intensity-weighted *B*, *V*, and *I* magnitudes.

[f] Luminosity amplitude in the *B*, *V*, and *I* band (mag).

[g] Variables whose *B* and *V* light curves were fitted with the Layden's template (Layden 1998).

[h] Variables that show *B* and *V* amplitude modulation.

TABLE 2

MEAN $B-V$ COLORS AND REDDENINGS FOR RR LYRAE STARS IN NGC 3201

ID (1)	$(B-V)_m$[a] (2)	$(B-V)_{\rm min}$[b] (3)	$E(B-V)_{\rm W90}$[c] (4)	$E(B-V)_{\rm PACZ}$[d] (5)	$(B-V)_{0,\rm PACZ}$[e] (6)
1	0.69	0.75	0.35	0.33	0.36
3[f]	0.69	0.75	0.36	0.34	0.35
4	0.69	0.77	0.37	0.34	0.35
5	0.61	0.70	0.33	0.29	0.32
7	0.65	0.71	0.31	0.27	0.38
8	0.70	0.74	0.34	0.32	0.38
9	0.64	0.72	0.35	0.31	0.33
13	0.69	0.78	0.40	0.34	0.35
17	0.62	0.70	0.32	0.27	0.35
19[f]	0.65	0.73	0.36	0.31	0.34
21	0.66	0.68	0.30	0.31	0.35
22	0.66	0.74	0.35	0.30	0.36
23	0.66	0.73	0.34	0.30	0.36
25	0.59	0.70	0.33	0.27	0.32
26[f]	0.70	0.77	0.39	0.37	0.33
28	0.67	0.77	0.39	0.33	0.34
31[f]	0.65	0.76	0.39	0.30	0.35
32	0.61	0.70	0.32	0.29	0.32
34[f]	0.57	0.67	0.31	0.27	0.30
35	0.67	0.72	0.33	0.30	0.37
36	0.55	0.65	0.29	0.22	0.33
37[f]	0.63	0.67	0.29	0.24	0.39
39	0.62	0.72	0.36	0.31	0.31
40	0.71	0.76	0.36	0.32	0.39
41	0.70	0.74	0.33	0.31	0.39
44	0.68	0.74	0.35	0.31	0.37
45	0.67	0.74	0.37	0.35	0.31
47[f]	0.56	0.61	0.24	0.19	0.37
49	0.64	0.74	0.35	0.30	0.34
51[f]	0.68	0.75	0.38	0.36	0.32
56	0.70	0.75	0.36	0.35	0.35
57	0.66	0.74	0.35	0.30	0.36
58[f]	0.70	0.75	0.35	0.33	0.37
71	0.68	0.75	0.36	0.32	0.36
73	0.65	0.76	0.39	0.33	0.32
77	0.63	0.70	0.32	0.28	0.35
78	0.63	0.66	0.29	0.28	0.35
80	0.64	0.72	0.33	0.29	0.35
83	0.62	0.71	0.33	0.29	0.33
90	0.64	0.71	0.32	0.29	0.35
2710	0.62	0.71	0.33	0.29	0.33

[a] Mean magnitude-weighted $B-V$ color.
[b] Mean color at minimum phase, i.e., $(0.5 \leq \Phi \leq 0.8)$.
[c] Reddening estimate based on the Sturch 1966 method according to the Walker's calibration (Walker 1990).
[d] Reddening estimate according to the PACZ relation (see text).
[e] Mean $B-V$ color dereddened using the PACZ relation.
[f] Variables that show B and V amplitude modulation.

Fourier series by adopting 15 components and estimating the typical Fourier coefficients. Columns (2) to (6) of Table 6 list the first Fourier amplitude, as well as amplitude ratios (R_{21}, R_{31}) and phase differences (ϕ_{21}, ϕ_{31}). Then we estimated the intrinsic mean $(B-V)_0$ and $(V-I)_0$ colors according to the empirical relations derived by KW01 and based on period as well as on A_1 and A_3 Fourier amplitudes (see their relations 6 and 9). The individual reddening evaluations based on these relations are given in columns (5) and (6) of Table 6. The new estimates soundly confirm previous findings, and indeed $E(B-V)$ values range from 0.24 (V36) to 0.35 (V13, V56), while the $E(V-I)$ values range from 0.30 [(V22, V36)] to 0.44 (V56). Moreover, the mean values we find are $\langle E(B-V)\rangle = 0.31 \pm 0.03$, and $\langle E(V-I)\rangle = 0.36 \pm 0.04$, respectively.

Although different methods based on mean $B-V$ and $V-I$ colors do supply similar reddening estimates, we decided to compare individual values to investigate whether they present any systematic drift with intrinsic color. Figure 10 shows the difference between current reddening evaluations based on the PACZ relation and the estimates based on the W90 relation (*top*), on the KW01 relation (*middle*), as well as on the ACZ relation (*bottom*). Data plotted in the top panel clearly show the systematic difference of $\approx$0.03 between the two methods (see § 5.1). On the other hand, data plotted in the middle and in the bottom panel clearly

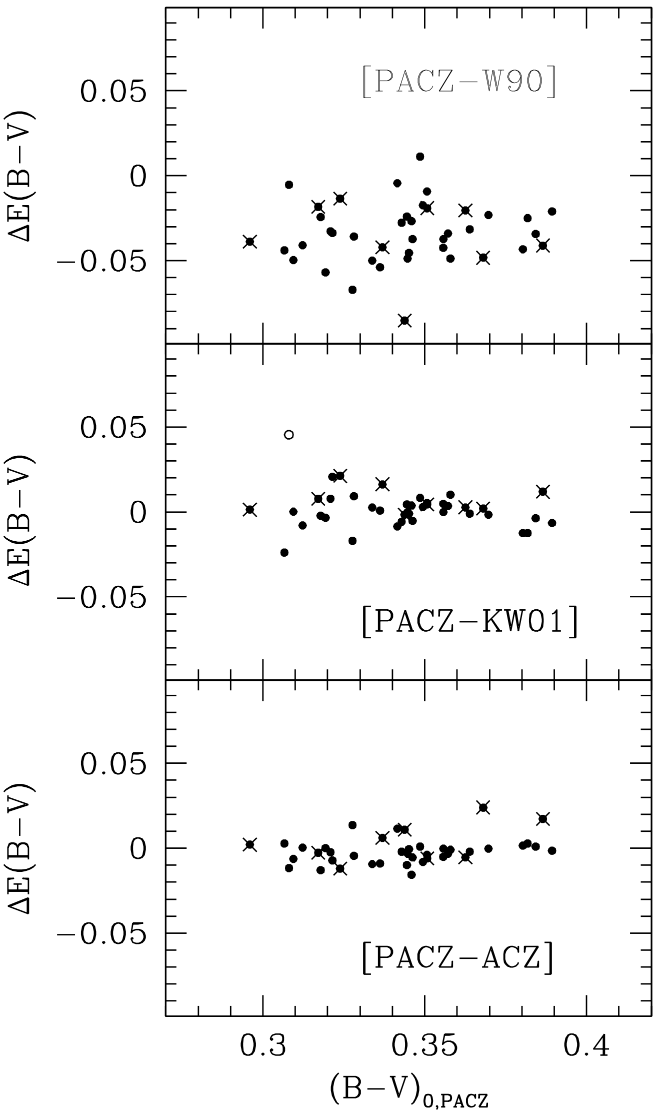

FIG. 10.—Difference for RR Lyrae stars in our sample between $E(B-V)$ color excesses estimated using the PACZ relation and the W90 relation (*top*), the KW01 relation (*middle*), as well as the ACZ relation (*bottom*). Variables that show amplitude modulation in the *B* and in the *V* band are marked with a cross. The open circle in the middle panel marks the position of the variable V45. Variables characterized by a poor phase coverage were not included.

indicate that the difference between the PACZ, the KW01, and the ACZ relations is negligible. However, data plotted in the middle panel seem to suggest that the scatter of individual measurements increases toward the blue edge of the instability strip. The relations derived by KW01 do rely on well-observed cluster RR Lyrae stars, and therefore this finding strengthens the accuracy of current relations and supplies and independent support to the KW01 relations.

Figure 11 shows the difference between current reddening determinations based on the PAC relation and the estimates based on the M95 (*top*) and on the KW01 (*bottom*) relation. A glance at the data plotted in the top panel seems to suggest that the M95 relation slightly underestimates reddening evaluations when compared with reddenings based on the PAC relation. According to current data sample it is not clear whether this discrepancy increases when moving

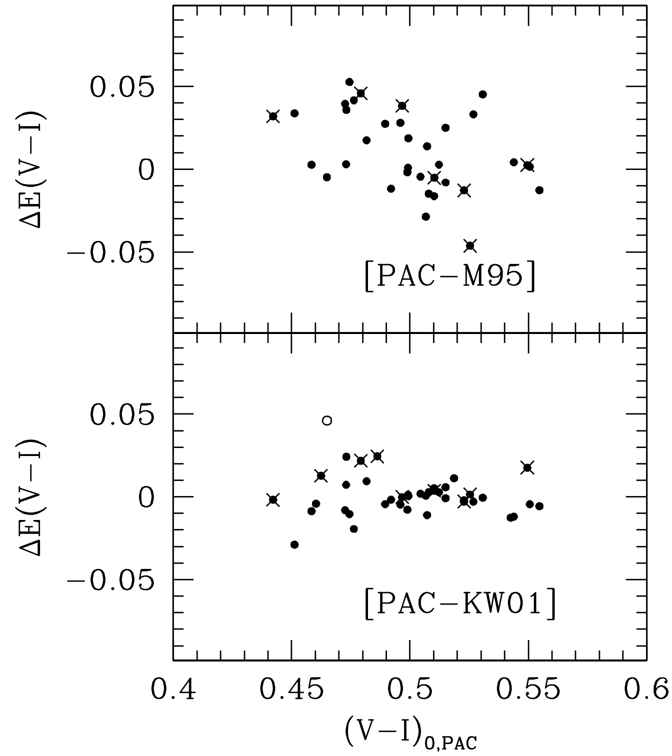

FIG. 11.—Same as Fig. 10, but the difference refers to the $E(V-I)$ color excesses estimated using the PAC relation and the M95 relation (*top*), as well as the KW01 relation (*bottom*). Symbols are the same as in Fig. 10.

toward the blue edge. On the other hand, data plotted in the bottom panel disclose that reddenings based on the PAC relation and on the KW01 relation are in very good agreement, within the uncertainties. The evidence that, close to the blue edge, the scatter of individual measurements between current and KW01 relations increases also applies to the $E(V-I)$-values. The variable V45 (*open circle*) presents a peculiar color excess; see the Appendix for more details.

6. COMPARISON BETWEEN THEORY AND OBSERVATIONS

To supply accurate estimate of the mean RR Lyrae magnitudes and colors in our sample, we performed a weighted mean between the $E(B-V)$ determinations obtained by adopting both the PACZ and the KW01 relation. The same approach was adopted to evaluate the mean $E(V-I)$, but according to the PAC and to the KW01 relation. Table 7 lists, from left to right, the identification, the dereddened *V* magnitude, $B-V$, and $V-I$ colors, together with the color excesses, namely, $E(B-V)$ and $E(V-I)$. The reddenings of RR*ab* stars whose light curve was fitted with the Layden's template are only based on the PACZ and the PAC relation. Magnitude and colors of RR*c* stars were dereddened by smoothing with a spline the reddening map derived using RR*ab* color excesses.

According to previous individual evaluations, $\langle V_0(\mathrm{RR})\rangle = \{\sum_{i=1}^{nr}([V(\mathrm{RR}) - 3.1 \times E(B-V)]\}/nr$, we estimated the apparent zero-age horizontal-branch (ZAHB) luminosity by adopting the relation originally suggested by Carney et al. (1992a) and revised by Cassisi & Salaris (1997,

TABLE 3

Reddening Determinations of Selected GGCS with RR Lyrae Stars

Cluster [a](1)	[Fe/H] [b](2)	$E(B-V)$ [c](3)	$\Delta E(B-V)$ [d](4)	$E(B-V)$ [e](5)	$E(V-I)$ [f](6)	RR*ab*[g] (7)	Ref.[h] (8)
NGC 1851	−1.36	0.02	0.02	0.04 ± 0.01	0.02 ± 0.01	7	1
NGC 4590/M68	−2.09	0.05	0.01	0.05 ± 0.01	0.06 ± 0.02	7	2
NGC 5466	−2.22	0.00	0.02	0.01 ± 0.01	...	7	3
NGC 5904/M5	−1.40	0.03	0.01	0.04 ± 0.03	0.05 ± 0.02	21, 33[i]	4, 5, 6, 7
NGC 6341/M92	−2.24	0.02	0.02	0.04 ± 0.02	...	6	8
NGC 6441	−0.5⋆	0.44	0.17	0.53 ± 0.14	...	15	9
NGC 7006	−1.59	0.05	0.03	0.01 ± 0.03	...	15	10
NGC 7089/M2	−1.62	0.06	−0.02	0.01 ± 0.01	...	12	11
Ruprecht 106	−1.7⋆	0.20	−0.03	0.15 ± 0.02	...	13	12

[a] Cluster name.

[b] Cluster metallicity according to ZW84. Clusters marked with a ⋆ are from Harris 1996.

[c] Cluster reddening based on light emitted by cluster members (Dutra & Bica 2000).

[d] Difference between the cluster reddening based on far-infrared dust emission (Schlegel et al. 1998) and the reddening listed in the previous column (Dutra & Bica 2000).

[e] Cluster reddening and standard deviation based on current B, V photometry and the PACZ relation.

[f] Cluster reddening and standard deviation based on current V, I photometry and the PAC relation.

[g] Number of fundamental RR Lyrae stars adopted to estimate the mean cluster reddening.

[h] Source of the photometry for cluster RR Lyrae stars: (1) Walker 1998, (2) Walker 1994, (3) Corwin, Carney, & Nifong 1999, (4) Storm et al. 1991, (5) Reid 1996, (6) Brocato et al. 1996, (7) Caputo et al. 1999, (8) Carney et al. 1992b, (9) Pritzl et al. 2001, (10) Wehlau, Slawson, & Nemec 1999, (11) Lee & Carney 1999, (12) Kaluzny, Krzeminski, & Mazur 1995.

[i] The former value refers to $B-V$ colors, while the latter to $V-I$ colors.

hereafter CS97), i.e., $V(\mathrm{ZAHB}) = \langle V(\mathrm{RR})\rangle + 0.04[\mathrm{M/H}] + 0.15$. The comparison between predicted ZAHB luminosities for $[\mathrm{M/H}] = -1.13$ (CS97) and empirical V magnitudes dereddened by adopting previous $E(B-V)$ evaluations supplies a distance modulus for NGC 3201 of $\mathrm{DM} = 13.30 \pm 0.08$ ($nr = 40$). Interestingly enough, if we adopt the visual ZAHB magnitudes dereddened by adopting the $E(V-I)$ determinations, $\langle V_0(\mathrm{RR})\rangle = \{\sum_{i=1}^{nr}[V(\mathrm{RR}) - 2.54 \times E(V-I)]\}/nr$, we find $\mathrm{DM} = 13.35 \pm 0.09$ ($nr = 35$). Figure 12 shows the comparison in the $V_0-(B-V)_0$ and in the $V_0-(V-I)_0$ CMD between predicted ZAHB magnitudes (*solid line*) and observed HB stars. The dashed line marks the exhaustion of central He burning. Predicted luminosities and effective temperature were transformed into the observational plane by adopting the bolometric corrections and the color-temperature relations by Castelli, Gratton, & Kurucz (1997).

Magnitudes and colors of HB stars plotted in Figure 12 were dereddened by adopting the same procedure adopted for RR*c* variables, and therefore they are the subsample of cluster HB stars located in the cluster region covered by current RR Lyrae sample. Data plotted in this figure clearly show that theoretical predictions for central He-burning structures are, within current

TABLE 4

The Main Pulsational Properties of Field RR*ab* Stars with *BVI* Data

ID	[Fe/H]	log P	$A(B)$	$\langle B-V\rangle$	$\langle V-I\rangle$	$A(V)$	$E(B-V)$	$E(V-I)$	Ref.[a]
SW And	−0.15	−0.35432	1.27	0.430	0.537	0.95	0.06	0.07	1
X Ari...........	−2.40	−0.1863	1.26	0.48	0.71	1.01	0.14	0.17	2
RR Cet.........	−1.25	−0.25725	1.21	0.366	0.525	0.93	0.03	0.04	1
UU Cet	−1.28	−0.2175	0.85	0.384	0.555	0.65	0.015	0.02	3
SU Dra	−1.6	−0.18018	1.26	0.344	0.512	0.97	0.01	0.01	1
SW Dra........	−1.12	−0.2444	1.15	0.36	0.515	0.90	0.015	0.02	4
RX Eri	−1.4	−0.23118	1.14	0.413	0.579	0.88	0.05	0.06	1
SS For..........	−0.94	−0.3050	1.65	0.30	0.45	1.3	0.015	0.02	4
RR Gem	−0.20	−0.40087	1.62	0.393	0.501	1.21	0.075	0.10	1
V Ind............	−1.50	−0.3191	1.35	0.338	0.488	1.05	0.015	0.02	3
RR Leo	−1.15	−0.34449	1.64	0.329	0.472	1.30	0.05	0.02	1
TT Lyn	−1.35	−0.22371	0.92	0.378	0.548	0.70	0.01	0.01	1
AV Peg.........	0.00	−0.40852	1.41	0.419	0.525	1.03	0.07	0.09	1
RV Phe	−1.69	−0.2245	0.90	0.37	0.53	0.65	0.015	0.02	4
TU Uma	−1.25	−0.25365	1.22	0.36	0.517	0.94	0.02	0.025	1
V440 Sgr	−1.40	−0.3235	1.6	0.40	0.55	1.2	0.12	0.15	4
W Tuc	−1.57	−0.1923	1.4	0.323	0.482	1.10	0.015	0.02	3
UU Vir.........	−0.55	−0.32275	1.5	0.335	0.440	1.17	0.01	0.01	1

[a] References: (1) Liu & Janes 1990; (2) Fernley et al. 1989; (3) Clementini, Cacciari, & Lindgren 1990; (4) Cacciari et al. 1987.

TABLE 5
MEAN $V-I$ COLORS AND REDDENINGS FOR RR LYRAE STARS IN NGC 3201

ID (1)	$(V-I)_{\rm m}$ [a] (2)	$(V-I)_{\rm min}$ [b] (3)	$E(V-I)_{\rm PAC}$ [c] (4)	$E(V-I)_{\rm M95}$ [d] (5)	$(V-I)_0$ [e] (6)
1	0.87	0.96	0.37	0.38	0.49
3[f]	0.93	1.01	0.42	0.43	0.50
4	0.94	1.04	0.43	0.46	0.48
5	0.78	0.90	0.32	0.32	0.44
8	0.83[g]	0.86	0.28[g]	0.28	0.53
9	0.78[g]	0.88	0.30	0.30[g]	0.46
13	0.82[g]	0.90	0.32	0.32[g]	0.49
17	0.84	0.90	0.34	0.32	0.50
21	0.84	0.93	0.33	0.35	0.51
22	0.82[g]	0.89	0.30	0.31[g]	0.51
23	0.87	0.91	0.35	0.33	0.52
25	0.81	0.86	0.33	0.28	0.48
26[f]	0.86	0.92	0.39	0.34	0.48
28	0.87	0.97	0.38	0.39	0.47
31[f]	0.91	0.95	0.41	0.37	0.51
32	0.87	0.94	0.40	0.36	0.46
34[f]	0.77	0.88	0.33	0.30	0.43
35	0.88	0.88	0.35	0.30	0.55
36	0.76[g]	0.82	0.28	0.24	0.49
37[f]	0.82	0.85	0.27	0.27	0.57
39	0.81	0.90	0.35	0.32	0.44
40	0.88[g]	0.91	0.33	0.33[g]	0.56
41	0.96	1.00	0.41	0.42	0.56
44	0.90	0.92	0.37	0.34	0.54
45	0.91	1.03	0.45	0.45	0.44
47[f]	0.72	0.79	0.20	0.21	0.51
49	0.80	0.86	0.31	0.28	0.49
56	0.96	1.02	0.44	0.44	0.51
58[f]	0.88	0.98	0.35	0.40	0.51
73	0.82[g]	0.84	0.36	0.26[g]	0.48
77	0.80	0.88	0.30	0.30	0.49
78	0.80[g]	0.86	0.31	0.28	0.50
80	0.89	0.95	0.38	0.37	0.51
83	0.89	0.96	0.42	0.38	0.47
90	0.82	0.90	0.32	0.32	0.49
2710	0.82	0.90	0.34	0.32	0.47

[a] Mean magnitude-weighted $V-I$ color.
[b] Mean color at minimum phase, i.e., $(0.5 \leq \Phi \leq 0.8)$.
[c] Reddening estimate based on the PAC relation.
[d] Reddening estimate based on the empirical evidence that for RR Lyrae stars $(V-I)_{0,\rm min} = 0.58 \pm 0.03$ mag (Mateo et al. 1995).
[e] Mean $V-I$ color dereddened according to the reddenings listed in the fourth and in the fifth column (weighted average).
[f] Variables that show B and V amplitude modulation.
[g] Variables that present larger photometric uncertainty.

uncertainties on reddening and distance estimates, in good agreement with observations. Stars located below the ZAHB with $0.4 \leq (B-V) \leq 0.5$ and $0.55 \leq V-I \leq 0.65$ colors should be field stars, and indeed a similar plume shows up just above the subgiant branch (see Fig. 15).

A few RR Lyrae stars are also located below the ZAHB, but they present a limited phase coverage or they are affected by amplitude modulation. Note that in the latter case current B and V amplitudes could be underestimated, and in turn the individual reddening corrections (see §§ 5.1 and 5.2).

The region of hot HB stars presents a larger spread in the $(V, V-I)$ than in the $(V, B-V)$ diagram. This is due to the fact that magnitudes and colors based on $E(V-I)$ determinations present larger errors than those based on $E(B-V)$ ones (see the error bars in Fig. 12).

Accurate distance moduli of globular clusters can be provided by adopting the method suggested by Caputo (1997). The match in the M_V-log P plane between predicted FO blue edge and the observed blue limit of RR*c* variables does supply an independent and robust estimate of the distance modulus (Caputo et al. 2000 and references therein). Unfortunately, the application of this method to NGC 3201 is hampered by the small number of RR*c* variables (five) as well as by the fact that we lack individual reddening estimates for these objects. However, to supply an independent check on the accuracy of current distance estimates, Figure 13 shows the comparison in the $(V, B-V)$ and in the $(V, V-I)$ plane between predicted instability edges for

TABLE 6

Fourier Parameters[a] and Reddening Estimates for RR Lyrae Stars in NGC 3201

ID[b] (1)	A_1[c] (2)	R_{21}[d] (3)	R_{31}[d] (4)	Φ_{21}[e] (5)	Φ_{31}[e] (6)	$E(B-V)$[f] (7)	$E(V-I)$[f] (8)	$(B-V)_0$[g] (9)	$(V-I)_0$[g] (10)
1	0.305	0.470	0.326	2.415	5.222	0.33	0.36	0.35	0.51
3[h]	0.283	0.458	0.310	2.419	5.279	0.34	0.42	0.35	0.51
4	0.333	0.555	0.325	2.636	5.512	0.34	0.43	0.35	0.51
5	0.442	0.430	0.304	2.136	4.828	0.30	0.33	0.30	0.45
7	0.193	0.360	0.109	2.132	6.025	0.28	...	0.37	0.53
8	0.207	0.387	0.199	2.820	5.891	0.33	0.30	0.37	0.53
9	0.357	0.553	0.316	2.320	4.850	0.31	0.30	0.33	0.48
11	0.269	0.196	0.067	3.024	5.982	...	...	...	...
13	0.323	0.538	0.329	2.620	5.460	0.35	0.32	0.34	0.50
17	0.311	0.503	0.310	2.340	5.058	0.27	0.34	0.34	0.50
19[h]	0.267	0.465	0.381	2.520	5.350	0.30	...	0.35	0.51
21	0.255	0.487	0.311	2.465	5.287	0.30	0.33	0.36	0.52
22	0.275	0.488	0.344	2.420	5.350	0.30	0.30	0.36	0.52
23	0.262	0.466	0.281	2.420	5.240	0.31	0.36	0.36	0.51
25	0.394	0.461	0.293	2.140	4.580	0.28	0.34	0.32	0.46
26[h]	0.337	0.619	0.375	2.656	5.678	0.35	0.36	0.34	0.50
28	0.360	0.522	0.321	2.346	4.997	0.33	0.38	0.34	0.49
31[h]	0.282	0.475	0.291	2.455	5.359	0.31	0.41	0.34	0.50
32	0.441	0.478	0.318	2.320	4.980	0.30	0.41	0.32	0.46
34[h]	0.443	0.441	0.295	2.292	4.833	0.27	0.33	0.30	0.44
35	0.224	0.476	0.276	3.020	5.230	0.30	0.35	0.37	0.53
36	0.356	0.395	0.209	2.290	4.882	0.24	0.30	0.31	0.46
37[h]	0.072	0.447	0.286	2.380	4.990	0.23	0.26	0.40	0.57
39	0.494	0.410	0.254	2.120	4.860	0.34	0.38	0.28	0.42
40	0.171	0.418	0.210	2.554	5.656	0.33	0.34	0.38	0.55
41	0.174	0.415	0.209	2.670	5.520	0.32	0.41	0.38	0.55
44	0.248	0.426	0.291	2.430	5.360	0.32	0.38	0.36	0.52
45	0.372	0.529	0.559	1.690	4.435	0.32	0.40	0.35	0.51
47[h]	0.143	0.116	0.067	0.886	3.102	0.19	0.20	0.37	0.52
48[h]	0.236	0.138	0.094	3.514	6.985	...	...	...	...
49	0.354	0.412	0.312	2.340	4.910	0.30	0.32	0.34	0.49
51[h]	0.401	0.576	0.373	2.340	4.870	0.35	...	0.32	0.48
56	0.304	0.504	0.388	2.394	5.150	0.35	0.44	0.36	0.52
57	0.249	0.483	0.395	2.420	5.190	0.30	...	0.37	0.53
58[h]	0.252	0.506	0.312	2.366	5.247	0.33	0.35	0.37	0.53
71	0.253	0.434	0.291	2.725	5.831	0.32	...	0.36	0.52
73	0.445	0.515	0.325	1.890	4.460	0.34	0.37	0.31	0.46
77	0.337	0.461	0.295	2.230	5.030	0.30	0.31	0.34	0.49
78	0.314	0.377	0.281	2.570	5.190	0.30	0.31	0.33	0.49
80	0.326	0.409	0.281	2.210	4.860	0.30	0.39	0.34	0.50
83	0.486	0.758	0.591	2.890	6.220	0.29	0.39	0.34	0.50
90	0.323	0.501	0.336	2.430	5.248	0.29	0.31	0.35	0.51
1405	0.211	0.090	0.051	2.834	3.130	...	...	...	...
2710	0.341	0.539	0.335	2.460	5.196	0.29	0.33	0.34	0.49

[a] Fourier parameters estimated by fitting V-band light curves (see text).
[b] Variable identification.
[c] First Fourier amplitude.
[d] Amplitude ratios: R_{21} between second and first harmonic, while R_{31} between third and first harmonic.
[e] Phase differences: ϕ_{21} between the second and first harmonic, while ϕ_{31} between the third and first harmonic.
[f] Reddening evaluations based on the KW relations (see text for more details).
[g] Mean $B-V$ and $V-I$ colors dereddened using the KW relations.
[h] Variables that show B and V amplitude modulation.

RR*ab* (*solid lines*) and RR*c* (*dashed lines*) pulsators (Bono et al. 2001 and references therein) and observed RR Lyrae stars in NGC 3201. Predicted edges were plotted by assuming a distance of DM $= 13.32$ and rely on full-amplitude, nonlinear, convective models constructed by adopting the same stellar mass ($M/M_\odot = 0.70$) and chemical composition ($Y = 0.24$, $Z = 0.0004$) and a wide range of stellar luminosities. Luminosities and effective temperatures were transformed into the observational plane by adopting the transformations by Castelli et al. (1997).

Note that the distribution of variable stars inside the instability strip is in good agreement with theoretical predictions. In fact, the red (cooler) edge properly marks the transition between RR*c* and RR*ab* variables. On the other hand, the RR Lyrae stars in the (V, $V-I$) plane appear slightly redder, thus supporting the evidence that we are

TABLE 7

DEREDDENED COLORS FOR THE ENTIRE SAMPLE OF RR LYRAE STARS

ID	V_0[a]	$(B-V)_0$[b]	$(V-I)_0$[c]	$E(B-V)$[d]	$E(V-I)$[d]
1	13.76	0.35	0.51	0.33	0.36
2[e]	13.98	0.34	0.48	0.27	...
3[f]	13.83	0.35	0.51	0.34	0.42
4	13.71	0.35	0.51	0.34	0.43
5	13.80	0.31	0.45	0.29	0.33
6[e,f]	13.74	0.31	0.45	0.30	...
7	13.82	0.38	0.54	0.27	...
8	13.71	0.38	0.54	0.32	0.29
9	13.81	0.33	0.48	0.31	0.30
11[g]	13.77	0.19	0.29	0.32	0.34
12[e]	13.74	0.32	0.46	0.34	...
13	13.75	0.35	0.50	0.35	0.32
17	13.90	0.35	0.50	0.27	0.34
18[e]	13.89	0.35	0.49	0.26	...
19[f]	13.79	0.35	0.50	0.31	...
20[e]	13.78	0.33	0.48	0.30	...
21	13.88	0.35	0.51	0.30	0.33
22	13.77	0.36	0.52	0.30	0.30
23	13.81	0.36	0.51	0.30	0.36
25	13.88	0.32	0.47	0.27	0.34
26[f]	13.77	0.34	0.49	0.36	0.38
28	13.78	0.34	0.49	0.33	0.38
31[f]	13.99	0.34	0.50	0.30	0.41
32	13.81	0.32	0.47	0.29	0.40
34[f]	13.91	0.30	0.44	0.27	0.33
35	13.79	0.37	0.53	0.30	0.35
36	14.00	0.32	0.47	0.23	0.29
37[f]	14.01	0.39	0.56	0.24	0.26
38[e,f]	13.88	0.33	0.47	0.29	...
39	13.78	0.30	0.44	0.32	0.37
40	13.77	0.38	0.55	0.33	0.33
41	13.83	0.39	0.55	0.32	0.41
44	13.77	0.37	0.53	0.31	0.37
45	13.83	0.33	0.49	0.33	0.42
47[f]	14.04	0.37	0.52	0.20	0.19
48[fg]	13.76	0.29	...	0.30	...
49	13.76	0.34	0.49	0.30	0.31
50[e]	13.86	0.36	0.47	0.24	...
51[f]	13.60	0.32	0.47	0.35	...
56	13.81	0.36	0.51	0.35	0.44
57	13.92	0.36	0.52	0.30	...
58[f]	13.68	0.37	0.53	0.33	0.35
71	13.69	0.36	0.52	0.32	...
73	13.69	0.31	0.46	0.34	0.36
76[e]	13.85	0.32	0.47	0.29	...
77	13.77	0.34	0.49	0.29	0.30
78	13.89	0.34	0.49	0.29	0.31
80	13.81	0.35	0.50	0.30	0.39
83	13.89	0.33	0.49	0.29	0.40
90	13.75	0.35	0.51	0.29	0.31
92[e]	13.77	0.33	0.48	0.30	......
1405[g]	13.85	0.28	0.36	0.29	0.36
2710	13.83	0.34	0.49	0.29	0.33

[a] Dereddened mean intensity-weighted V magnitude. The adopted reddening correction is the average between the PACZ and the KW relation.

[b] Dereddened mean $B-V$ color according to PACZ and KW relation.

[c] Dereddened mean $V-I$ color according to PAC and KW relation.

[d] Reddening correction based on current and KW relations (weighted mean).

[e] Variables whose B and V light curves were fitted using the Layden's template (Layden 1998).

[f] Variables that show B and V amplitude modulation.

[g] RR*c* pulsator for which the reddening was derived using the reddening map of RR*ab* star.

slightly underestimating the reddening in this plane. Intrinsic colors of RR*c* variables should be treated cautiously, since their reddenings are based on the RR*ab* reddening map and are therefore affected by uncertainties of the order of $E(V-I) \approx 0.04$. The metallicity adopted for the instability edges ([Fe/H] $= -1.65$) is more metal-poor than that adopted for HB models ([Fe/H] $= -1.42$, i.e., [M/H] $= -1.13$). The comparison between empirical data and predicted edges for $Z = 0.001$ shows the same agreement. The main difference is that a good fraction of RR*ab* variables moves into the "OR" region. Unfortunately, the sample of RR*c* variables is too small to draw any firm conclusion concerning the topology of the instability strip and the mean metallicity.

The luminosity amplitudes are robust observables to constrain the physical parameters governing the pulsation properties of radial variables. In fact, they are not affected by empirical uncertainties in the distance modulus, and they are marginally affected by errors in reddening evaluations. Figure 14 displays the comparison in the Bailey diagram between current sample of RR Lyrae variables with RR Lyrae stars in M5 (*open circles*) and in IC 4499 (*open squares*). We selected these two clusters because they have almost the same metallicity and host a sizable sample of RR Lyrae stars. Data plotted in this figure indicate that RR Lyrae stars in these three clusters do show similar distributions in the Bailey diagram. In particular RR*ab* variables cover the same period range and attain similar luminosity amplitudes when moving from the blue to the red edge of the instability strip. The number of RR*c* variables in NGC 3201 is too small to draw any conclusion concerning the occurrence of a systematic difference in the period distribution.

Data plotted in Figure 14 clearly support the finding originally brought out by Smith (1981) that *irregular variability is more frequent among fundamental pulsators with periods shorter than 0.65 days*. As a matter of fact, the spread in the luminosity amplitudes becomes substantially smaller for $\log P \geq -0.2$. Together with empirical data Figure 14 shows the comparison with predicted *B*-, *V*-, and *I*-band amplitudes. Theoretical observables are based on the same models we adopted in Figure 13. Predicted amplitudes for $\log L/L_\odot = 1.61$ and 1.72 bracket empirical data and suggest a luminosity for RR Lyrae stars in NGC 3201 of the order of $\log L/L_\odot = 1.65$. This pulsational estimate agrees, within current uncertainties on chemical composition, with the luminosities predicted by HB models when moving from [Fe/H] $= -1.25$ to [Fe/H] $= -1.65$, i.e., $1.63 \leq \log L/L_\odot \leq 1.68$. Finally, we note that empirical amplitudes for RR*ab* stars do show, at fixed period, a large scatter inside the instability strip.

However, the RR Lyrae stars in NGC 3201 that show amplitude modulation are located at the bottom of this distribution. This finding supports the evidence that the observed scatter could be due to RR Lyrae stars that undergo amplitude modulations.

7. THE COLOR-MAGNITUDE DIAGRAM

The top panels of Figure 15 show the (V, $B-V$) and (V, $V-I$) diagrams. The effect of the differential reddening is quite evident in the (V, $V-I$) diagram, and indeed in this plane the stars along the RGB split over two distinct sequences. This notwithstanding, the CMDs show a well-

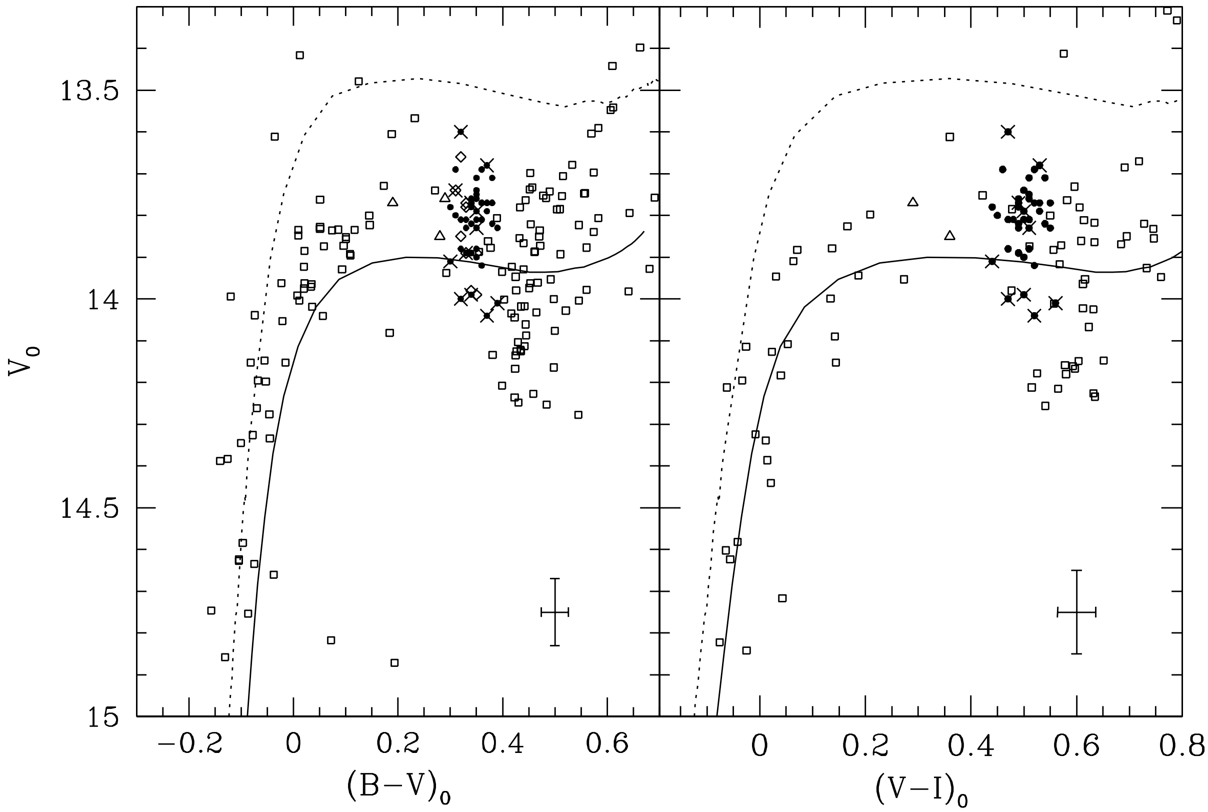

FIG. 12.—Comparison in the V_0, $(B-V)_0$ (*left*) and in the V_0, $(V-I)_0$ (*right*) CMD between theory and observations. The solid line shows the ZAHB, while the dashed line the exhaustion of central He burning for [M/H] $= -1.13$. Theoretical predictions were plotted by adopting a distance modulus of 13.32 ± 0.06. HB stars and RR*c* variables were dereddened by smoothing with a spline the reddening maps based on RR*ab* stars. The error bars display the uncertainties on magnitude and colors due to errors on individual reddening estimates. Symbols are the same as in Fig. 5; open squares display HB stars.

defined main sequence (MS) at least down to $V \approx 20.5$ and well-populated post-MS phases together with a sequence of blue stragglers approaching hot HB stars. Data plotted in this figure are the average of more than 70 measurements in each band. We only plotted stars with photometric errors in the three bands smaller than 0.02. The bottom panels of Figure 15 display the extinction corrected V_0 magnitudes versus $(B-V)_0$ and $(V-I)_0$ obtained by adopting the reddening maps based on RR*ab* stars. The number of stars in the bottom panels is smaller than in the top ones, since we only plotted stars located inside current reddening maps. The resolution of these maps is of the order of $1'$. The plausibility of the reddening correction is supported by the narrowing of the main evolutionary phases.

The CMD of NGC 3201 presents several similarities with the CMD of M3, and indeed the fiducial lines derived by Ferraro et al. (1997) for this cluster overlap to dereddened data for NGC 3201 (*bottom left*, Fig. 15). The main discrepancy between the two cluster data sets is among extreme HB stars. This mismatch could be due to the calibration of the photometric zero point (see Ferraro et al. 1997 for further details). At the same time we also note that the $B-V$ color of our standard stars do not cover extreme HB stars. This notwithstanding, data plotted in this figure show very good agreement between the RGB mean loci of M3 and individual RGB stars in NGC 3201. This evidence supports the zero point of current reddening scale as well as individual reddenings, since M3 is only marginally affected by reddening $[E(B-V) \approx 0.01]$. A further interesting similarity between M3 and NGC 3201 is a sizable sample of blue stragglers (CO97). The properties of these stars will be addressed in forthcoming paper. The same outcome applies to the dereddened (V, $V-I$) CMD, and indeed data plotted in the bottom right panel show a very good agreement between the mean ridge line provided by Johnson & Bolte (1998) and current photometry. Note that the agreement applies not only to TO and RGB regions but also to hot and cool HB stars.

A thorough discussion concerning the evolutionary properties of this cluster will be addressed in a forthcoming paper. In this context we briefly discuss the RGB bump. This interesting evolutionary feature appears as a peak in the differential luminosity function (LF) and as a change in the slope of the cumulative LF. From an evolutionary point of view, the presence of such a bump is due to the fact that during the RGB evolution the H-burning shell crosses the chemical discontinuity left over by the convective envelope soon after the first dredge-up at the base of the RGB. We located the RGB bump in NGC 3201 using both the differential and the cumulative LFs and we find $V_{\rm bump} = 14.55 \pm 0.05$ mag. The comparison between theory and observations concerning the location of the bump along the RGB is a crucial test to assess the accuracy of current evolutionary models. Dating back to Fusi Pecci et al. (1990) it became clear that the $\Delta V_{\rm HB}^{\rm bump}$, i.e., the difference in magnitude between the RGB bump and the HB stars located inside the RR Lyrae instability strip, is the key parameter to compare theory and observations.

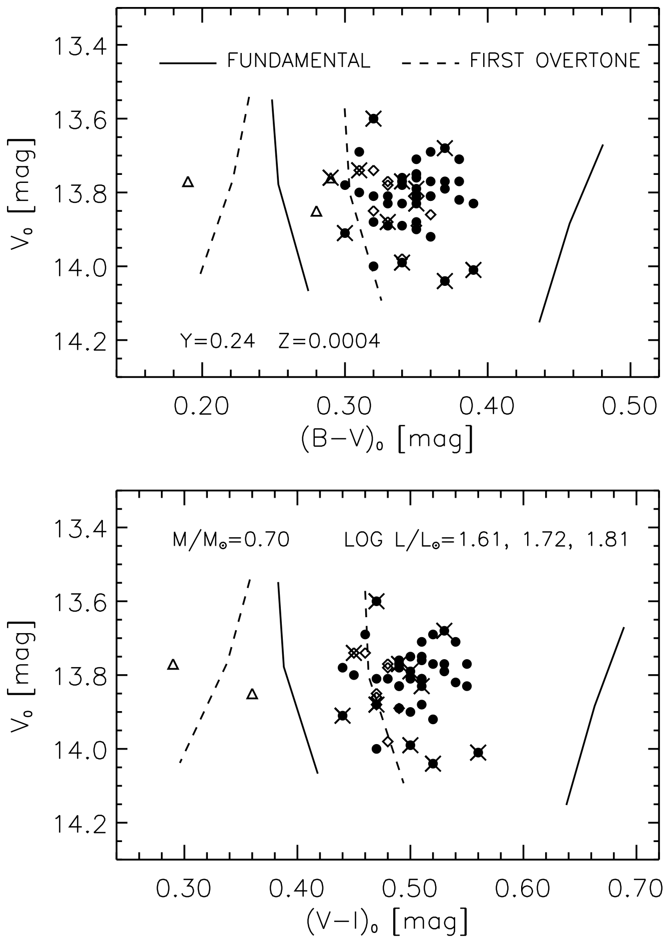

FIG. 13.—Same as Fig. 12, but for RR Lyrae variables. Solid and dashed lines show predicted fundamental and first-overtone instability edges respectively. Adopted stellar mass and chemical composition are labeled. The comparison was performed by adopting a distance modulus of 13.32 ± 0.06. Symbols are the same as in Fig. 5.

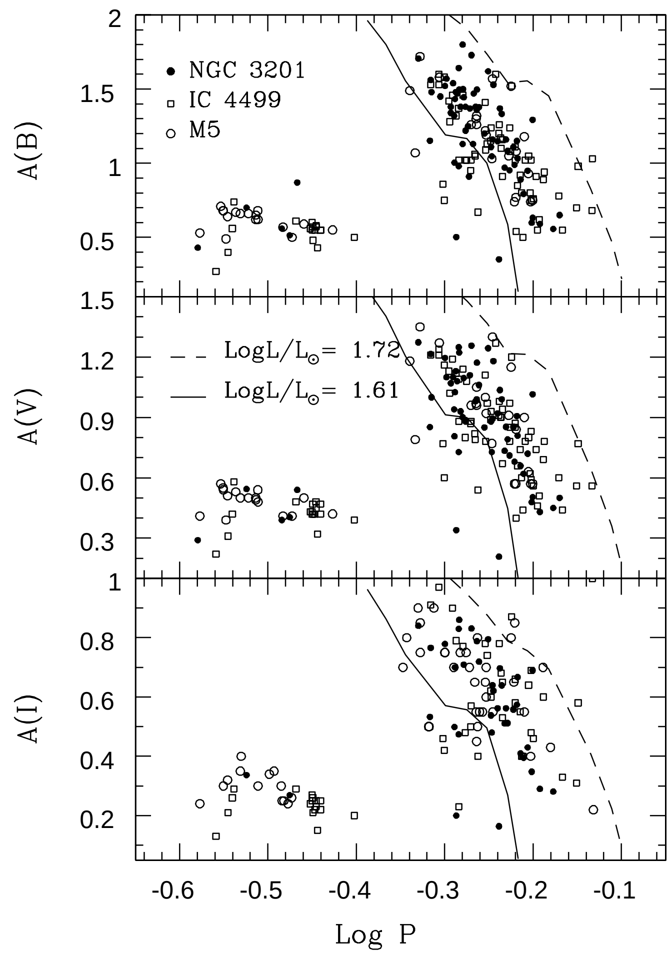

FIG. 14.—*Top*: Comparison in the Bailey diagram between RR Lyrae stars in NGC 3201 in M5 (*open circles*) and in IC 4499 (*open squares*), respectively. Solid and dashed lines display predicted amplitudes for pulsation models constructed by adopting different luminosity levels (see labeled values). *Middle*: Same as top, but for *V* amplitudes. Note that top and the middle panels show five RR*c* stars, since we also included the two extra RR*c* variables observed by C84. *Bottom*: Same as top, but for *I* amplitudes.

To estimate this parameter, we adopted current RR Lyrae sample, and we find a mean magnitude of $\langle V_{\rm RR} \rangle = 14.75 \pm 0.07$. This magnitude was scaled to the ZAHB luminosity according to the correction suggested by CS97, and eventually we find $V_{\rm ZAHB} = 14.85 \pm 0.07$ mag. Therefore, the $\Delta V_{\rm HB}^{\rm bump}$ for NGC 3201 is equal to -0.30 ± 0.09 mag. Figure 16 shows the comparison between this value and theoretical predictions (CS97). Note that for NGC 3201 we adopted the mean global metallicity based on the spectroscopic measurements of iron and α-elements given by GW98 and the relation between global metallicity, iron abundance, and α-element enhancements provided by Salaris et al. (1993). For the aim of the comparison, the same figure also shows empirical estimates of $\Delta V_{\rm HB}^{\rm bump}$ for a selected sample of GGCs for which accurate spectroscopic measurements of iron and α-element enhancement are available (see labeled names). Theoretical predictions rely on evolutionary models at fixed initial He content ($Y = 0.23$, Zoccali et al. 2000) that cover a wide range of progenitor masses ($M/M_\odot = 0.8$–1.0) and global metallicities ($-2.3 \le [{\rm M/H}] \le -0.5$). Data plotted in this figure show that theory and observations are in fine agreement. The empirical value of $\Delta V_{\rm HB}^{\rm bump}$ for NGC 3201 seems slightly smaller than predicted by theoretical models. This finding, taken at face value, could suggest that the mean global metallicity of this cluster is slightly more metal-poor than currently estimated.

8. SUMMARY AND CONCLUSIONS

We present *BVI* time-series data of NGC 3201 collected over three consecutive nights, which cover a cluster region of approximately 13 arcmin^2 around the center. Current data allowed us to identify 72 out of the 104 variables or suspected variables originally detected by SH73, Lee (1977), and Welch & Stetson (1993). According to current data we confirm the nonvariability for 10 of them and strongly support the evidence brought out by GW98 that V79 is a red variable located close to the tip of the RGB. The light curves of RR Lyrae stars in our sample (53) present a very good phase coverage. The only exception to this rule are nine RR Lyrae stars with periods close to 0.5 days that present a poor phase coverage close to the phases of maximum/minimum luminosity.

The comparison between current data and photographic data collected by SH73 and C84 support the evidence that

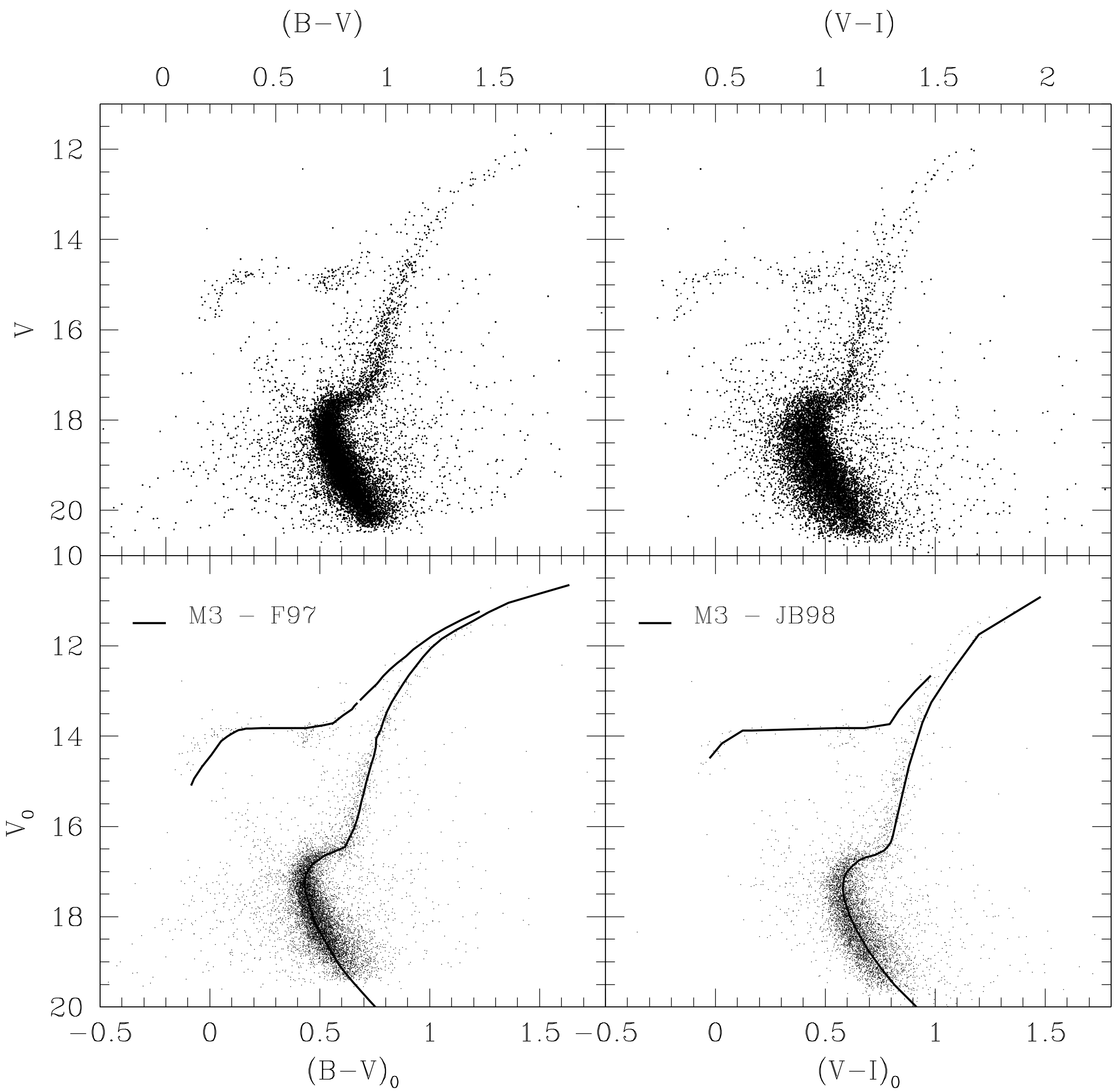

FIG. 15.—Reddened (*top*) and dereddened (*bottom*) (V, $B-V$) and (V, $V-I$) CMDs. Individual reddening evaluations were obtained by adopting the reddening maps based on RR*ab* colors. As a consequence, the bottom panels only display the subsample of cluster stars located inside these maps. Note the substantial decrease in the thickness of RGB stars, as well as in the subgiant and in the turnoff region. The solid lines in the bottom panels show the fiducial lines for M3 according to Ferraro et al. (1997; V, $B-V$) and Johnson & Bolte (1998; V, $V-I$). To overplot the two sets of fiducial lines we applied a magnitude shift of -1.85 and -1.8, respectively.

approximately the 30% of RR*ab* variables present amplitude modulation (the Blazhko effect). This result supports the findings originally brought out by Szeidl (1976) and Smith (1981) for field and cluster RR Lyrae stars. At the same time we confirm that RR*ab* that show the Blazhko effect present periods shorter than 0.65 days (Smith 1981). We also find that one (V48) out of the three RR*c* variables is strongly suspected to be affected by amplitude modulation. If new data confirm this evidence, this object would be the first cluster RR*c* variable that shows such a phenomenon.

To overcome the thorny problem of differential reddening across the cluster, we derived new empirical relations connecting the intrinsic $B-V$ and $V-I$ colors of RR Lyrae stars with pulsation parameters. By adopting a large sample of field RR Lyrae stars (78) for which B amplitude, $B-V$ color, metallicity are available and which present a low reddening or accurate reddening estimate, we find that they do obey an ACZ and a PACZ relation. The key features of these relations are the following: (1) They depend on stellar parameters that are not affected by reddening. (2) They supply accurate estimates of intrinsic $B-V$ colors across the fundamental instability region and cover a wide metallicity range. This means that they can be used to estimate the reddening of halo and bulge RR Lyrae stars. (3) They have been derived by neglecting the RR Lyrae stars that present or are suspected to be affected by amplitude modulation. To validate the zero point of the reddening scale, we applied the new relations to the large sample of RR Lyrae stars (207) in M3 recently collected by Corwin & Carney (2001). We selected this RR Lyrae sample since the reddening toward this cluster is vanishing [$E(B-V) \approx 0.01$]. We find that both the ACZ and the PACZ relations account for the mean cluster reddening, but the intrinsic scatter of the latter one is somehow smaller. Moreover and even more importantly, we find that the difference in the mean cluster reddening based on an RR Lyrae sample that includes or neglects

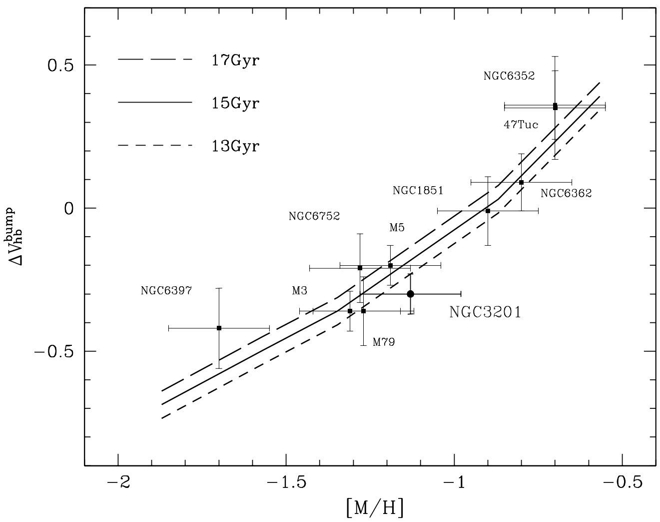

FIG. 16.—Comparison between predicted and empirical $\Delta V_{\rm HB}^{\rm bump}$ values as a function of global metallicity. Long-dashed, solid, and dashed lines show theoretical predictions for three different cluster ages (see labeled values). To avoid systematic uncertainties that could affect current metallicity scales (Rutledge et al. 1997), we only plotted GGCs for which are available spectroscopic measurements of iron and α-element abundances.

Blazhko RR Lyrae stars is marginal. This finding suggests that previous relations can be safely adopted to estimate the reddening of well-sampled Blazhko RR Lyrae stars.

We adopted the same approach to derive a relation that allow us to derive individual reddening on the basis of the $V-I$ colors. We selected a sample of 18 field plus 49 cluster (IC 4499, NGC 6362) RR*ab* variables for which are available V amplitude, $V-I$ color, metallicity, and accurate reddening estimates. Interestingly enough, we find that they do obey to a PAC relation; i.e., the metallicity term is vanishing. This means that this relation can be used to estimate the reddening on the basis of period and mean $V-I$ color. Unfortunately, we could not validate the zero point of this relation, since I-band data are not available for RR Lyrae stars in M3, and we are not aware of GGCs with a large sample of RR Lyrae stars, vanishing reddening, and accurate $V-I$ colors. However, the comparison between the mean reddenings based on the PAC and on the PACZ relation for clusters for which *BVI* data are available shows a good agreement within the uncertainties.

We applied the PACZ relation to fundamental RR Lyrae stars in our sample and by assuming a mean cluster metallicity of $[\mathrm{Fe/H}] = -1.42$ we find $\langle E(B-V)\rangle = 0.30 \pm 0.03$, while the individual reddening estimates range from 0.22 (V36) to 0.35 (V45). The intrinsic scatter we find $[\Delta E(B-V) \approx 0.15]$ is slightly larger than estimated by GW98 on the basis of 17 RGB stars. However, it is worth noting that the current estimate agrees with the mean value obtained by adopting the dust infrared map by SFD98. As a matter of fact, on the same cluster region we find a mean reddening of $\langle E(B-V)\rangle = 0.26 \pm 0.02$. Note that the angular resolution of the SFD98 map is approximately $6'$, while our map has a resolution of the order of $1'$.

The same outcomes apply to the PAC relation, and indeed we find a mean cluster reddening of $\langle E(V-I)\rangle = 0.36 \pm 0.05$, while the individual reddening estimates range from 0.28 (V36) to 0.45 (V45). The spread between individual evaluations support the results by vBM01, who found that the differential reddening across the cluster changes by approximately 0.2 mag. On the other hand, current mean cluster reddening is larger than the mean reddening obtained using the reddening map by vBM01 on the same cluster region $[\langle E(V-I)\rangle = 0.25 \pm 0.07]$. However, our evaluation based on $V-I$ colors is internally consistent with the mean reddening based on the $B-V$ colors, $\langle E(V-I)\rangle = 1.22)\rangle \times \langle E(B-V)\rangle = 0.37 \pm 0.04$ and, in turn, with the SFD98 map.

We performed a detailed comparison with similar relations available in the literature and found that current relations are in very good agreement with the reddening estimates based on the relations derived by KW01. In fact, the KW01 relations supply mean cluster reddenings of $\langle E(B-V)\rangle = 0.31 \pm 0.03$ and of $\langle E(V-I)\rangle = 0.36 \pm 0.04$. These relations have been calibrated using cluster RR Lyrae stars for which are available BV- and I-band data and rely on Fourier amplitudes and periods. The main advantage of current relations is that they can also be applied to RR Lyrae stars with limited phase coverage. However, the ACZ and the PACZ relations require knowledge of the metallicity, while the KW01 relations and the PAC relation only rely on periods and luminosity amplitudes.

To supply a detailed comparison between theory and observations, we dereddened the magnitudes of the stars located inside current reddening maps. The comparison between predicted ZAHB luminosities for He-burning structures located inside the instability strip and observed RR Lyrae stars provides a distance modulus of 13.30 ± 0.08 if we adopt the V magnitudes dereddened using the $E(B-V)$ map. Interestingly enough, we find that the distance modulus is 13.35 ± 0.09 if the V magnitudes are dereddened using the $E(V-I)$ map, and therefore the weighted true distance modulus is 13.32 ± 0.06. This estimate is in good agreement with values available in the literature and based on different distance indicators (see CO97 for a detailed discussion). However, the uncertainty affecting current distance determination is smaller than similar estimates. The main difference is due to the fact that we are adopting individual reddenings and not a mean cluster reddening. However, previous errors do not account for current uncertainties on predicted ZAHB luminosities ($\approx$0.1 mag, see e.g., Cassisi et al. 1999; Bono, Castellani, & Marconi 2000) or on mean cluster metallicity. An uncertainty of 0.2 dex in the mean metallicity implies an uncertainty on the distance modulus given by predicted ZAHB luminosities of the order of 0.05 mag. It goes without saying that the K-band period-luminosity-metallicity relation of RR Lyrae stars should overcome these problems, since it presents a mild dependence on cluster metallicity as well as on individual reddenings (Bono et al. 2001).

The current RR Lyrae sample covers a cluster region that is approximately one-third of the cluster tidal radius ($r_t = 28\farcm5$, Harris 1996[9]). New multiband time-series data collected with a wide-field imager would be extremely useful to extend current reddening maps and to increase their angular resolution. This is mandatory to improve the intrinsic accuracy of the CMD and, in turn, the empirical evaluations of cluster parameters. Finally, we also mention that new CCD data are also necessary to estimate the secondary

[9] See http://physun.mcmaster.ca/~harris.

period of RR Lyrae stars affected by amplitude modulation and therefore to constrain on a quantitative basis the occurrence and the intimate nature of the Blazhko effect.

It is a pleasure to thank S. Covino for sending us *BV* data of cluster stars and G. Clementini for *BVI* data of field RR Lyrae variables. We also thank S. Cassisi and M. Marconi for providing us evolutionary and pulsational predictions in advance of publication. We wish also to acknowledge an anonymous referee for his/her detailed suggestions and helpful comments, which improved both the content and the readability of this paper. We are grateful to G. Kovacs for sending us his code for the Fourier analysis, F. Caputo for a critical reading of an early draft of this manuscript, C. Cacciari and L. Pulone for useful discussions on photometric calibrations, and M. Dolci for enlightening suggestions concerning IDL routines. This work was supported by MURST/COFIN 2000 under the project Stellar Observables of Cosmological Relevance.

APPENDIX

COMMENTS ON INDIVIDUAL VARIABLES

V6: Our data do not cover the phases around minimum light. Therefore current amplitude estimates, which are larger than the estimates by C84, are uncertain. However, the light curve published by L02 supports the hypothesis that this object presents an amplitude modulation (the Blazhko effect), since our V magnitude close to the maximum light is roughly 0.2 mag brighter than measured by L02. The difference seems real since current calibration does agree with the calibration provided by L02.

V19: The difference in the luminosity amplitudes between current and C84 estimates (about 0.3 mag) suggests that this variable is a Blazhko candidate. However, the light curve given by C84 does not show a well-defined maximum, and therefore the amplitude is slightly uncertain.

V23: The light curve of this object is presented here for the first time. Both the period (recomputed) and the amplitudes agree quite well with the estimates provided by L02.

V26: It is a good Blazhko candidate since the difference in the B amplitude between current and C84 estimate is of the order of 0.35 mag. The position of this object in the Bailey plane is also peculiar and supports previous hypothesis.

V31: The difference between current and C84 B amplitude is quite large and roughly equal to 0.6 mag. However, the amplitude provided by C84 is affected by a large uncertainty, and therefore the change might not be real.

The comparison between current mean V magnitude and the mean magnitude provided by C84 shows that the latter one is 0.12 mag brighter. This evidence suggest that it might be a blend in the C84 photometry.

V36: The period of this object was estimated and the new value is 0.482143 days, while the old one was 0.4757433 (C84). However, current and C84 amplitudes do agree within the errors.

Moreover, the comparison between current mean V magnitude and the mean magnitude provided by C84 shows that the latter one is 0.2 mag brighter. This evidence suggests that it might be a blend in the C84 photometry (see her Table IV).

V37: This variable is the reddest object [$(B-V)_0 \approx 0.40$ mag] in our sample and presents a very low luminosity amplitude ($A_B = 0.35$). According to its position in the CM diagram, it could be located close to the red edge, but its period is 0.577 days, while several RR*ab* stars present periods longer than 0.62 days.

However, the reddening correction for this variable increases from $E(B-V) = 0.24$ to $E(B-V) = 0.27$ if we adopt the B amplitude estimated by C84 ($A_B = 0.97$ mag). This change might account for previous peculiarities, since V37 becomes slightly bluer and roughly 0.1 mag brighter. This object is a candidate Blazhko RR Lyrae stars.

V41: The light curve of this object is presented here for the first time. The new period 0.6650 days is quite similar to the estimate provided by SH73 (0.66 days).

V45: This variable is the object for which the dereddened colors derived through the KW01 relations present the largest discrepancy with current estimates. The difference could be due to our Fourier amplitudes. In fact, the Fourier series do not properly fit the light curve around the minimum. Unfortunately, this variable is not included in the C84 sample, and therefore we cannot assess whether it presents any peculiarity in the luminosity amplitude.

V47: We estimated the period of this variable and we found that the new value $P = 0.5164$ days is quite similar to the period derived by C84, i.e., $P = 0.5212$ days. We also found an alternative period of 0.3414 days, but the shape of the light curve (see Fig. 17) is typical of a RR*ab* star. However, current amplitude ($A_B = 0.50$) is too small for a RR*ab* with this period. This peculiarity suggests that this object might be a Blazhko RR Lyrae stars and supports the former classification by SH73 and C84.

V48: It is one of the two first-overtone variables in common with C84 and the difference in the B amplitude is larger than 0.3 mag. However, current and C84 light curves are affected by a large scatter. This empirical evidence, once confirmed, would imply that V48 is the first cluster RR*c* that shows the Blazhko effect.

V51: The difference between current and C84 B amplitude is quite large, but its light curve presents a large scatter, probably because it is located close to the edge of the frame. The evidence that this variable is affected by the Blazhko effect is not firm.

V58: The difference between current and C84 B amplitude is roughly 0.4 mag, and the phase coverage along the light curves is good. This variable is a good candidate to be a Blazhko RR Lyrae star.

Note that this object is somehow peculiar, and indeed the current mean V magnitude is 0.15 mag brighter than the mean magnitude provided by C84.

V50, V76, V80, V90, V92, V1405, V2710: The light curves of these objects are presented here for the first time. Their periods are: 0.5338, 0.52577, 0.588, 0.6024, 0.54047, 0.3346, 0.548 days.

V79: The B magnitude changes roughly from 13.7 to 13.6, while the V magnitude changes from 12.19 to 12.11 (see Fig. 18). We note that the variability of this object was also suggested by GW98. The location of this variable in the CMD suggests that it could be a semiregular variable. Unfortunately, the time interval covered by our observations does not allow us to estimate the pulsation period.

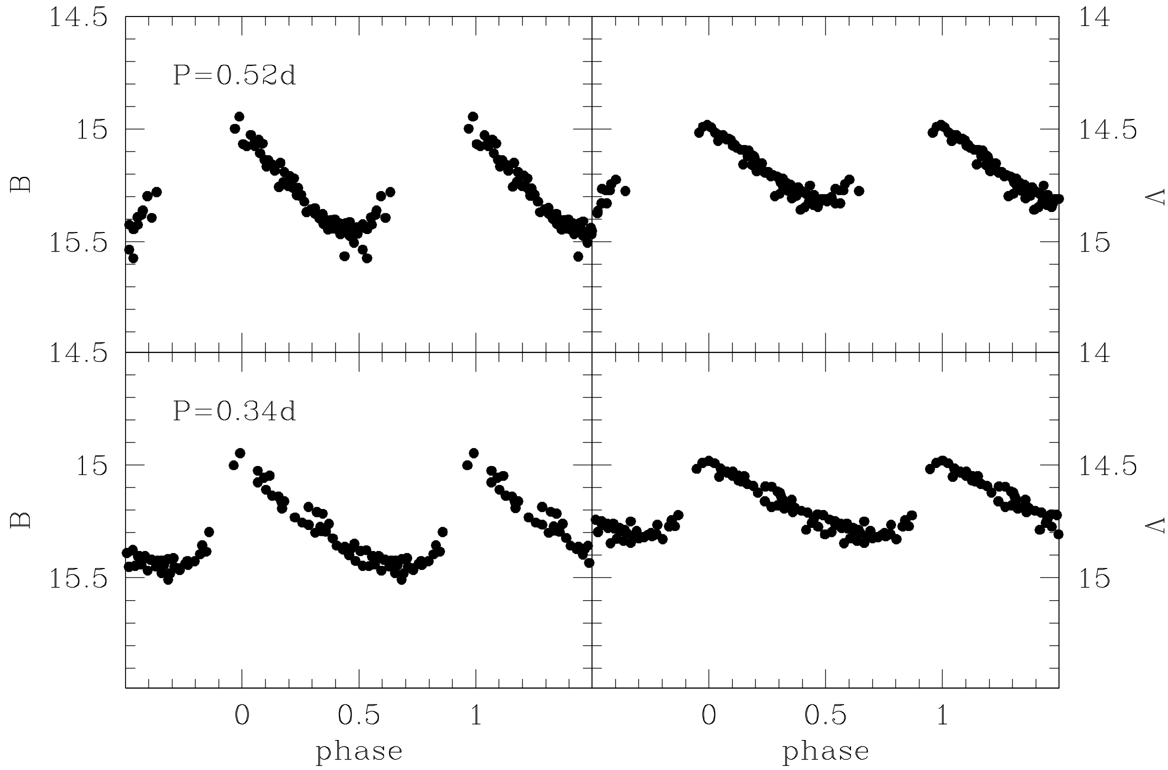

FIG. 17.—*B*- (*left*) and *V*- (*right*) band light curves of V47 phased by adopting two different periods, namely, 0.5164 and 0.3414 days

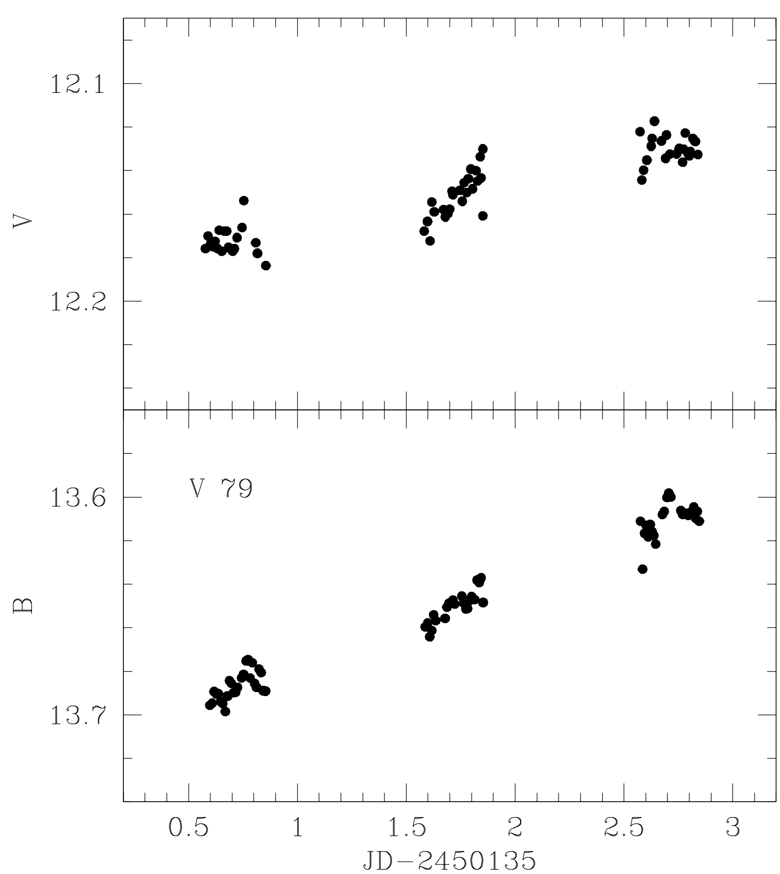

FIG. 18.—*V* (*top*) and *B* (*bottom*) magnitudes as a function of the Julian day for the suspect red variable V79. This object is located close to the tip of the RGB.

REFERENCES

Alard, C. 1999, A&A, 343, 10
———. 2000, A&AS, 144, 363
Albrow, M. D., Gilliland, R. L., Brown, T. M., Edmonds, P. D., Guhathakurta, P., & Sarajedini, A. 2001, ApJ, 559, 1060
Alcaino, G., & Liller, W. 1981, AJ, 86, 1480
Alcaino, G., Liller, W., & Alvarado, F. 1989, A&A, 216, 68
Andersen, M. I., Freyhammer, L., & Storm, J. 1995, in ESO/ST-ECF Workshop on Calibrating and Understanding HST and ESO Instruments, ed. P. Benvenuti (Garching: ESO), 87
Anthony-Twarog B. J., & Twarog, B. A. 2000, AJ, 119, 2282
Arce, H. G., & Goodman, A. A. 1999, ApJ, 517, 264
Bessel M. S. 1979, PASP, 91, 589
Blazhko, S. 1907, Astron. Nachr., 175, 325
Bono, G. Caputo, F., Cassisi, S., Castellani, V., & Marconi, M. 1997a, ApJ, 483, 811
———. 1997b, ApJ, 489, 822
Bono, G., Caputo, F., Castellani, V., & Marconi, M. 1997c, A&AS, 121, 327
Bono, G., Caputo, F., Castellani, V., Marconi, M., & Storm, J. 2001, MNRAS, 326, 1183
Bono, G., Castellani, V., & Marconi, M. 2000, ApJ, 532, L129
Bono, G., et al. 2002, in preparation
Bono, G., & Stellingwerf, R. F. 1994, ApJS, 93, 233
Borissova, J., Catelan, M., & Valchev, T. 2001, MNRAS, 324, 77
Bragaglia, A., et al. 2000, in IAU Colloq. 176, The Impact of Large-Scale Surveys on Pulsating Star Research, ed. L. Szabados & D. Kurtz (San Francisco: ASP), 271
Brewer, J., Fahlman, G., Richer, H., Searle, L. & Thompson, I. 1993, AJ, 105, 2158
Brocato, E., Castellani, V., & Ripepi, V. 1996, AJ, 111, 809
Cacciari, C. 1984, AJ, 89, 231 (C84)
Cacciari, C., Clementini, G., Prevot, L., Lindgren, H., Lolli, M., & Oculi, L. 1987, A&AS, 69, 135
Caputo, F. 1997, MNRAS, 284, 994
———. 1998, A&A Rev., 9, 33
Caputo, F., Castellani, V., Marconi, M. & Ripepi, V. 1999, MNRAS, 306, 815
———. 2000, MNRAS, 316, 819
Caputo, F., & De Santis, R. 1992, AJ, 104, 253 (CDS92)
Cardelli, J. A., Clayton, G. C., & Mathis, J. S. 1989, ApJ, 345, 245
Carney, B. W. 1996, PASP, 108, 900
Carney, B. W., Storm, J., & Jones, R. V. 1992a, ApJ, 386, 663
Carney, B. W., Storm, J., Trammell, S. R., & Jones, R. V. 1992b, PASP, 104, 44
Carretta, E., & Gratton, R. 1997, A&AS, 121, 95 (CG97)
Cassisi, S., Castellani, V., degl'Innocenti, S., Salaris, M., & Weiss, A. 1999, A&AS, 134, 103
Cassisi, S., Castellani, V., degl'Innocenti, S., & Weiss, A. 1998, A&AS, 129, 267
Cassisi, S., & Salaris, M. 1997, MNRAS, 285, 593 (CS97)
Castellani, V. 1999, in Globular Cluster, ed. C. Martinez Roger, I. Perez Fournon, & F. Sanchez (Cambridge: Cambridge Univ. Press), 109
Castelli, F., Gratton, R. G., & Kurucz, R. L. 1997, A&A, 324, 432
Clement, C. M., et al. 2001, AJ, 122, 2587
Clementini, G., Cacciari, C., & Lindgren, H. 1990, A&AS, 85, 865
Corwin, T. M., & Carney, B. W. 2001, AJ, 122, 3183
Corwin, T. M., Carney, B. W., & Nifong, B. G. 1999, AJ, 118, 2875
Covino, S., & Ortolani, S. 1997, A&A, 318, 40 (CO97)
Da Costa, G. S., Frogel, J. A., & Cohen, J. G. 1981, ApJ, 248, 612
D'Antona, F., Caloi, V., & Mazzitelli, I. 1997, ApJ, 477, 519
Dutra, C. M., & Bica, E. 2000, A&A, 359, 347 (DB00)
Edmonds, P. D., Heinke, C. O., Grindlay, J. E., & Gilliland, R. L. 2002, ApJ, 564, L17
Fernley, J. 1993, A&A, 268, 591
Fernley, J. A., Lynas-Gray, A. E., Skillen, I., Jameson, R. F., Marang, F., Kilkenny, D., & Longmore, A. J. 1989, MNRAS, 236, 447
Ferraro, F. R., Carretta, E., Corsi, C. E., Fusi Pecci, F., Cacciari, C., & Buonanno, R., Paltrinieri, B., & Hamilton, D. 1997, A&A, 320, 757
Fusi Pecci, F., Ferraro, F. R., Crocker, D. A., Rood, R. T., & Buonanno, R. 1990, A&A, 238, 95
Feuchtinger, M. U. 1999, A&AS, 136, 217
Gonzales G., & Wallerstein G. 1998, AJ, 116, 765 (GW98)
Harris, W. E. 1976, AJ, 81, 1095
———. 1996, AJ, 112, 1487
Jurcsik, J., & Kovacs, G. 1996, A&A, 312, 111
Johnson, J. A., & Bolte, M. 1998, AJ, 115, 693
Kaluzny, J., Krzeminski, W., & Mazur, B. 1995, AJ, 110, 2206
Kaluzny, J., Olech, A., & Stanek, K. Z. 2001, AJ, 121, 1533
Kaluzny, J., & Thompson, I. B. 2001, A&A, 373, 899
Kovacs, G. 1995, A&A, 295, 693
Kovacs, G., & Kanbur, S. M. 1998, MNRAS, 295, 834
Kovacs G., & Walker A. R. 2001, A&A, 371, 579 (KW01)
Kraft, R. P., Sneden, C., Langer, G. E., Shetrone, M. D., & Bolte, M. 1995, AJ, 109, 2586
Kurtz, D. W., et al. (The MACHO Collaboration). 2000, in IAU Colloq. 176, The Impact of Large-Scale Surveys on Pulsating Star Research, ed. L. Szabados & D. Kurtz (San Francisco: ASP), 291
Kurucz R. L. 1992, in IAU Symp. 149, The Stellar Populations of Galaxies, ed. B. Barbuy & A. Renzini (Dordrecht: Kluwer), 225
Layden, A. C. 1998, AJ, 115, 193
Layden, A. C., Cool, A., von Hippel T., & Sarajedini, A. 2002, in IAU Colloq. 185, Radial and Nonradial Pulsations as Probes of Stellar Physics, ed. C. Aerts, T. Bedding, & J. Christensen-Dalsgaard (San Francisco: ASP), 122 (L02)
Lee, J. W., & Carney, B. W. 1999, AJ, 117, 2868
Lee, S. W. 1977, A&AS, 28, 409
Liu, T., & Janes, K. A. 1990, ApJ, 354, 273
Lub, J. 1977, A&AS, 29, 345
———. 1979, AJ, 84, 383
Mateo, M., Udalski, A., Szymanski, M., Kaluzny, J., Kubiak, M., & Krzeminski, W. 1995, AJ, 109, 588 (M95)
Nagy, A. 1998, A&A, 339, 440
Olech, A., Kaluzny, J., Thompson, I. B., Pych, W., Krzeminski, W., & Schwarzenberg-Czerny, A. 2001, MNRAS, 321, 421
Olech, A., Wozniak, P. R., Alard, C., Kaluzny, J., & Thompson, I. B. 1999, MNRAS, 310, 759
Preston, G. W. 1964, ARA&A, 2, 23
Pritzl, B. J., Smith, H. A., Catelan, M., & Sweigart, A. V. 2001, AJ, 122, 2600
Reid, N. 1996, MNRAS, 278, 367
Roberts, W. J., & Grebel, E. K. 1995, A&AS, 109, 313
Rosenberg, A., Saviane, I., Piotto, G., & Aparicio, A. 1999, AJ, 118, 2306
———. 2000, A&AS, 144, 5
Rutledge, G. A., Hesser, J. E., & Stetson, P. B. 1997, PASP, 109, 907
Salaris, M., Chieffi, A., & Straniero, O. 1993, ApJ, 414, 580
Samus, N. N., et al. 1996, Astron. Lett., 22, 239
Sandage, A. 1990a, ApJ, 350, 603
———. 1990b, ApJ, 350, 631
Sawyer-Hogg, H. 1973, Publ. David Dunlap Obs., 3, No. 6 (SH73)
Schlegel, D. J., Finkbeiner, D. P., Davis, M. 1998, ApJ, 500, 525 (SFD98)
Schwarzschild, M. 1940, Cir. Harvard Coll. Obs., 437
Shibahashi, H. 2000, in IAU Colloq. 176, The Impact of Large-Scale Surveys on Pulsating Star Research, ed. L. Szabados & D. Kurtz (San Francisco: ASP), 291
Simon, N. R., & Clement, C. M. 1992, ApJ, 395, 192
Smith, H. A. 1981, PASP, 93, 721
Smith, H. A., Barnett, M., Silbermann, N. A., & Gay, P. 1999, AJ, 118, 572
Smith, H. A., & Manduca, A. 1983, AJ, 88, 982
Smith, H. A., Matthews, J. M., Lee, K. M., Williams, J., Silbermann, N. A., & Bolte, M. 1994, AJ, 107, 679
Stetson, P. B. 1987, PASP, 99, 191
———. 1995, DAOPHOT II User's Manual (Victoria: Dominion Astrophys. Obs.)
———. 2000, PASP, 112, 925
Storm, J., Carney, B. W., & Beck, J. A. 1991, PASP, 103, 1264
Sturch, C. 1966, ApJ, 143, 774
Szeidl, B. 1976, in IAU Coll. 29, Multiply Periodic Variable Stars, ed. W. S. Fitch (Dordrecht: Reidel), 133
———. 1988, in Multimode Stellar pulsations, ed. G. Kovacs, L. Szabados, & B. Szeidl (Budapest: Konkoly Obs.), 45
Trager, S. C., Djorgovski, S., & King, I. R. 1993, in Structure and Dynamics of Globular Clusters, ed. S. G. Djorgovski & G. Meylan (San Francisco: ASP), 347
Vandenberg, D. A. 2000, ApJS, 129, 315
Vandenberg, D. A., & Irwin, A. W. 1997, in Advances in Stellar Evolution (Cambridge: Cambridge Univ. Press), 22
Vandenberg, D. A., Stetson, P. B., & Bolte, M. 1996, ARA&A, 34, 461
van den Bergh, S. 1993, ApJ, 411, 178
van Hoolst, T. 2000, in IAU Colloq. 176, The Impact of Large-Scale Surveys on Pulsating Star Research, ed. L. Szabados & D. Kurtz (San Francisco: ASP), 307
von Braun K., & Mateo, M. 2001, AJ, 121, 1522 (vBM01)
Walker, A. R. 1990, AJ, 100, 1532 (W90)
———. 1994, AJ, 108, 555
Walker, A. R. 1998, AJ, 116, 220
Walker, A. R., & Nemec, J. M. 1996, AJ, 112, 2026
Wehlau, A., Slawson, R. W., & Nemec, J. M. 1999, AJ, 117, 286
Welch, D. L., & Stetson P. B. 1993, AJ, 105, 1813
Zinn, R. 1980, ApJS, 42, 19
Zinn, R., & West M. J. 1984, ApJS, 55, 45 (ZW84)
Zoccali, M., Cassisi, S., Bono, G., Piotto, G., Rich, R. M., & Djorgovski, S. G. 2000, ApJ, 538, 289